Biofabrication

International Society for Biofabrication

PAPER • **OPEN ACCESS**

Hyaluronic acid based next generation bioink for 3D bioprinting of human stem cell derived corneal stromal model with innervation

To cite this article: Anni Mörö *et al* 2023 *Biofabrication* **15** 015020

View the article online for updates and enhancements.

You may also like

- 3D bioprinted extracellular vesicles for tissue engineering—a perspective
Pingping Han and Sašo Ivanovski
- 3D coaxial bioprinting: process mechanisms, bioinks and applications
Tarun Shyam Mohan, Pallab Datta, Sepehr Nesaei et al.
- 3D bioprinting of mature bacterial biofilms for antimicrobial resistance drug testing
Evita Ning, Gareth Turnbull, Jon Clarke et al.

BREATH® BIOPSY

Breath Biopsy® OMNI

The most advanced, complete solution for global breath biomarker analysis

SEE WHAT OMNI CAN DO FOR YOU

Expert Study Design & Management

Robust Breath Collection

Reliable Sample Processing & Analysis

In-depth Data Analysis

Specialist Data Interpretation

This content was downloaded from IP address 130.230.32.174 on 17/01/2023 at 14:19

IOP Publishing Biofabrication 15 (2023) 015020 https://doi.org/10.1088/1758-5090/acab34

Biofabrication

PAPER

Hyaluronic acid based next generation bioink for 3D bioprinting of human stem cell derived corneal stromal model with innervation

Anni Mörö[1,*], Sumanta Samanta[2], Laura Honkamäki[3], Vignesh K Rangasami[2], Paula Puistola[1], Maija Kauppila[1], Susanna Narkilahti[3], Susanna Miettinen[4,5], Oommen Oommen[2] and Heli Skottman[1]

[1] Eye Regeneration Group, Faculty of Medicine and Health Technology, Tampere University, Tampere 33520, Finland
[2] Bioengineering and Nanomedicine Lab, Faculty of Medicine and Health Technology, University, Tampere 33720, Finland
[3] Neuro Group, Faculty of Medicine and Health Technology, Tampere University, Tampere 33520, Finland
[4] Adult Stem Cell Group, Faculty of Medicine and Health Technology, Tampere University, Tampere 33520, Finland
[5] Research, Development and Innovation Centre, Tampere University Hospital, Tampere 33520, Finland
[*] Author to whom any correspondence should be addressed.

E-mail: anni.moro@tuni.fi

Keywords: 3D bioprinting, bioink, cornea, human stem cells, innervation

Supplementary material for this article is available online

OPEN ACCESS

RECEIVED
15 November 2022

ACCEPTED FOR PUBLICATION
13 December 2022

PUBLISHED
29 December 2022

Original content from this work may be used under the terms of the Creative Commons Attribution 4.0 licence.

Any further distribution of this work must maintain attribution to the author(s) and the title of the work, journal citation and DOI.

Abstract

Corneal transplantation remains gold standard for the treatment of severe cornea diseases, however, scarcity of donor cornea is a serious bottleneck. 3D bioprinting holds tremendous potential for cornea tissue engineering (TE). One of the key technological challenges is to design bioink compositions with ideal printability and cytocompatibility. Photo-crosslinking and ionic crosslinking are often used for the stabilization of 3D bioprinted structures, which can possess limitations on biological functionality of the printed cells. Here, we developed a hyaluronic acid-based dopamine containing bioink using hydrazone crosslinking chemistry for the 3D bioprinting of corneal equivalents. First, the shear thinning property, viscosity, and mechanical stability of the bioink were optimized before extrusion-based 3D bioprinting for the shape fidelity and self-healing property characterizations. Subsequently, human adipose stem cells (hASCs) and hASC-derived corneal stromal keratocytes were used for bioprinting corneal stroma structures and their cell viability, proliferation, microstructure and expression of key proteins (lumican, vimentin, connexin 43, α-smooth muscle actin) were evaluated. Moreover, 3D bioprinted stromal structures were implanted into *ex vivo* porcine cornea to explore tissue integration. Finally, human pluripotent stem cell derived neurons (hPSC-neurons), were 3D bioprinted to the periphery of the corneal structures to analyze innervation. The bioink showed excellent shear thinning property, viscosity, printability, shape fidelity and self-healing properties with high cytocompatibility. Cells in the printed structures displayed good tissue formation and 3D bioprinted cornea structures demonstrated excellent *ex vivo* integration to host tissue as well as *in vitro* innervation. The developed bioink and the printed cornea stromal equivalents hold great potential for cornea TE applications.

1. Introduction

Corneal transplantation is considered as the most frequent type of tissue transplantation. It restores visual function and provides acceptable quality of life for the patients with severe forms of cornea blindness [1]. However, there is a dire shortage of donor corneas globally, leaving millions of visually impaired patients without treatment. This has given rise to vast research interest on developing tissue-engineered (TE) corneal substitutes that could mimic human cornea features and subsequently be used as an alternative for human donor cornea transplantations. Unfortunately, this challenge remains yet to be accomplished due to the extreme difficulty in mimicking the highly complex ultrastructure of the corneal stroma. To this day, none of the obtained TE cornea substitutes manufactured with the conventional scaffold-based approaches have been fully able to replicate the complexity as well as functionality with successful innervation [2].

© 2022 The Author(s). Published by IOP Publishing Ltd

3D bioprinting offers the best potential to engineer artificial tissues and organs among the myriad biofabrication techniques explored to date [3]. It allows precise spatial placement of cells into constructs mimicking complex and irregular shapes of the native tissue. Previously, human cornea stroma mimicking structures have been 3D bioprinted with extrusion-based printing [4], laser-assisted 3D bioprinting [5] as well as stereolithography [6]. While 3D bioprinting holds tremendous potential for fabrication of cornea mimicking structures, the current technological approaches have focused in merely in the 3D macro shapes bypassing the fine-tuned architecture of the cornea [7]. To the best of our knowledge there are limited studies that reported the bioprinting of microstructure of cornea. Kim *et al* induced shear stress to a cornea-stroma derived decellularized extracellular matrix bioink in extrusion-based printing to align collagen fibrils and to mimic the microstructure of the cornea stroma [8]. Sorkio *et al* used laser-assisted 3D bioprinting to print alternatively thin layers of cell-containing and acellular layers of bioink to mimic the lamellar structure of cornea stroma [5]. Despite the enormous potential of this emerging technology, there are still technological challenges limiting its wider use in cornea TE.

Hydrogel precursors with the ability to be extruded through a small-sized nozzle and subsequently forming shape-stable gels are suitable bioink components for extrusion-based printing [3]. Hyaluronic acid (HA) is a natural polysaccharide, which can be chemically modified for many TE applications, while being enzymatically cleared *in vivo* [9]. However, pure HA has poor mechanical properties resulting in limited structural support [10]. This could be circumvented by chemical modified of the polymer to improve its cytocompatibility and mechanical properties for wider use in TE applications [11]. One common form of chemically modified HA used in bioinks is methacrylated hyaluronic acid (HAMA), which could be photo-crosslinked resulting in enhanced printability and structural stability [12, 13]. Previously, HAMA bioinks have been successfully printed into scaffolds for soft and hard TE applications [14, 15]. In addition, 3D printed HA-modified gelatin methacrylate (GelMA-HA) scaffolds have been used as a substrate for rabbit corneal stromal cells [16]. However, post-treatment process of HAMA and GelMA-HA requires photoinitiators and photo-crosslinking, which can possess limitations on biological functionality [17, 18]. To date, HAbased bioinks without photo-crosslinking has not been used for 3D bioprinting of human cornea stromal equivalents.

Click chemistry-based hydrogels are formed spontaneously by mixing reactive compounds and can encapsulate live cells with high viability for long time [19]. Generally, these reactions are fast, spontaneous, versatile and extremely selective [20]. Existing bioinks that rely on ionic crosslinking, photo-crosslinking, or thermogelation have significantly advanced the field. Nevertheless, they have technical limitations in terms of the mechanics, swelling characteristics, degradation rates, and the cell viabilities achievable with the printed scaffolds [21]. Conventionally, azide-alkyne cycloaddition reaction, Diels–Alder reaction and thiol-ene chemistry are termed as click-chemistry owing to the biorthogonal nature of the reactive components and the atom economic reaction products. However, these methods are not ideal for fabricating bioinks for 3D printing with living cells as they require stringent reaction conditions, toxic catalyst, or high temperature. Hydrazone crosslinking is a fast and efficient pseudo click reaction formed by the dynamic covalent coupling between biorthogonal functional groups, namely aldehyde- and hydrazide-groups [22]. HA-based hydrazone crosslinked hydrogels have been previously studied for TE of cornea mimicking structures [23, 24]. However, the gelation time of the hydrazone crosslinking of HA-based hydrogels is fast (<30 s) resulting in narrow biofabrication window and therefore these hydrogels could not be used as a bioink for 3D bioprinting [24]. To date, relatively few examples of click chemistry based bioinks for extrusion printing have been reported [21]. Wang *et al* demonstrated extrusion-based bioprinting of hydrazone crosslinked HA using large 18 G needles [25]. In that study, smaller needles resulted in decreased cell viability. Thus, novel bioinks that provide ideal biofabrication window, high resolution and cell viability is greatly needed for extrusion-based 3D bioprinting. Such bioinks could be tailored using dynamic covalent chemistry that are fast and efficient and do not require any catalyst or light source.

Another key parameter for successful translation of 3D printed structures is innervation followed by integration to the host tissue, which are generally overlooked in most TE applications [26]. Implanted TE constructs typically lack preformed neuronal connections and rely on host-induced innervation. The cornea is the most densely innervated peripheral tissue in the body exhibiting a complex nerve architecture, distribution, and structural organization [27]. Previously, innervation of TE corneas has been demonstrated in simple 3D *in vitro* models where human cornea keratocytes, human cornea epithelial cells and rat ganglion cells are manually combined by stacking a few alternative layers of thin silk films and rat collagen type 1 hydrogel [28]. On the other hand, 3D bioprinting approaches of human pluripotent stem cell derived neuronal cells (hPSC-neurons) have utilized gelatin [29], fibrin [30, 31] and Matrigel/alginate [32] based bioinks with extrusion printing. These studies have focused on bioink development and cell viability of hPSC-neurons after printing. Thus, the full potential of utilizing 3D bioprinting

to create human stem cell based innervated corneal structures is yet to be explored.

To address these needs, we developed a HA-based bioink with hydrazone crosslinking for 3D bioprinting of human cornea stroma equivalents. Herein, we demonstrate that the developed hydrogel fulfills the requirements for next generation bioinks including excellent printability, shape fidelity as well as cytocompatibility with human adipose stem cells (hASC), hASC-derived corneal stromal keratocytes (hASC-CSKs) and hPSC-neurons. Moreover, we investigated several 3D bioprinting strategies for cornea stroma generation and analyzed the microstructure of the resulting stromal equivalents. We elaborated our studies by displaying tissue integration of the 3D bioprinted cornea stroma in a porcine corneal organ culture model. Finally, to demonstrate the utility of the developed bioink and 3D bioprinted cornea stroma, we explored the innervation to the printed cornea stroma as well as manufactured the first 3D bioprinted cornea stromal tissue model with innervation.

2. Materials and methods

2.1. Synthesis and characterization of the bioink components

Four bioink components were synthesized for this study. Grafting of dopamine to hyaluronic acid (HA-DA) was done as previously described [24]. The degree of dopamine modification was ascertained by Shimadzu UV-3600 plus UV–vis–NIR spectrophotometer at 275 nm against the standard curve prepared over a concentration range of 50–400 μM by dissolving commercial dopamine hydrochloride in phosphate buffered saline (PBS). Additionally, the conjugation of dopamine on the HA was further verified by attenuated total reflectance Fourier transform infrared (ATR-FTIR) spectroscopy by scanning the materials in the range of 4000–650 cm^{-1} with 32 scans at a resolution of 4 cm^{-1}. The conjugation of carbodihydrazide (CDH) on hyaluronic acid (HA-CDH) was carried out by carbodiimide coupling chemistry and the percentage hydrazide conjugation was determined by trinitrobenzene sulfonic acid (TNBS) assay [33]. The same hydrazide conjugation protocol was followed to conjugate CDH on dopamine-modified hyaluronic acid (HA-DA-CDH). The synthesis of HA-Aldehyde (HA-Ald) was conducted as previously described [34]. We recorded the proton nuclear magnetic resonance (^{1}H-NMR) spectra of synthesized HA-DA and HA-Ald at 298 K in D_2O using Zeol ECZR 500 instrument to validate and quantify the degree of modifications of dopamine and aldehyde respectively. The synthesized, HA-CDH, HA-DA-CDH and HA-Ald components were sterilized with UV for 20 min and dissolved into sterile PBS at a concentration of 10 mg ml^{-1}.

2.2. Preparation of the bioinks

In this study, we prepared two HA-based hydrazone-crosslinked bioinks to evaluate the effect of conjugated dopamine on the bioink characteristics. The first bioink contained HA-CDH and HA-Ald as crosslinking components (HA bioink) and the other HA-DA-CDH and HA-Ald (HA-DA bioink). Unmodified sodium hyaluronate (Novamatrix, Norway) was used as a primary rheological modifier and fully dissolved in sterile 5× PBS with 0.4 M NaCl at a concentration of 1% (w/v). The OptiCol™ Human Collagen Type I (Cell Guidance Systems Ltd, Cambridge, UK) was added to the bioink to gain better cytocompatibility and to act as an additional rheological modifier. Human Collagen Type I was neutralized to a pH of 7.4 with 1 M NaOH in the presence of 10× Dulbecco's phosphate buffered saline (Carl Roth, Karlsruhe, Germany). The final bioinks consisted of HA-CDH (HA bioink) or HA-DA-CDH (HA-DA bioink) and both supplemented with HA-Ald, rheological modifiers and cell culture medium in ratios 10:10:10:4, respectively. The mixing of the components was done using a dual syringe system, where two syringes were combined with a female–female Luer lock. After thorough mixing, the bioink was placed in a 30 cc Nordson EFD syringe barrel (Ohio United States), and the cartridge piston was placed in the barrel immediately. The bioink was allowed to crosslink at room temperature (RT) for 60 min before printing.

2.3. Injectability and shear-thinning/self-healing properties

To determine the injectability and shear-thinning property of the HA and HA-DA bioinks, we measured the viscosity and flow property of both bioinks under continuous flow (0.01–10 s^{-1}), and with a periodic shear rate of 0.01 and 10 s^{-1} up to seven cycles with 60 s of holding time for each cycle using 12 mm stainless-steel parallel plate geometry in TA instruments' DHR-II rheometer. To further evaluate the strain recovery of the fully crosslinked hydrogels, storage modulus (G′) and loss modulus (G″) was measured under alternating low (1%) and high oscillation strain (50%) conditions at 25 °C and 1 Hz oscillation frequency for seven cycles with 60 s of holding period in each step using 12 mm diameter stainless-steel parallel plate geometry.

2.4. 3D bioprinting setup

Here, we used extrusion-based 3D bioprinting with 3D-Bioplotter® Manufacturer Series by EnvisionTEC (Gladbeck, Germany). The barrel with a bioink was loaded into the low temperature printhead of the 3D bioprinter. About 32 G blunt needles (CellInk, Sweden, Gothenburg) with length of 0.50 inch and innerdiameter of 100 μm were used for printing. The printhead temperature was adjusted at 20 °C and the printing was carried out at RT. 3D models in stl format were created with Perfactory RP Software

(EnvisionTEC, Gladbeck, Germany) and the inner parameters including printing patterns were adjusted in Visual Machine (EnvisionTEC, Gladbeck, Germany) 80 μm slice interval was used for all printed structures, and needle height at first layer was adjusted at 0.07 mm.

2.5. Printability

The effect of the covalent grafting of dopamine component on the bioink printability was evaluated. For this, HA and HA-DA bioinks were printed with two different printing parameters, 0.8 bar and 15 mm s^{-1} and 1.0 bar 6 mm s^{-1}. Grid structures of two layers with dimensions of 20 mm $\times$ 20 mm were printed. Distance between filaments in each layer was set at 2.0 mm. Images were taken after every printed layer with a high-definition charged coupled-device (CCD)-camera attached to the dispense head mount to evaluate the printability and filament formation of the two bioinks.

2.6. Shape fidelity

The stacking ability of the 3D printed HA-DA bioink was investigated by printing 3D cylinders with a diameter of 13 mm and height of 1 mm, consisting of 13 printed layers. The line distance used was 400 μm and the alternative layers were set in 90° angle. The stacking ability of the resulting 3D structure was evaluated visually. For further exploring the shape fidelity of the HA-DA bioink, the filament thickness and pore factor (Pr) of printed structures was measured as a function of time in multilayered structures. For this, HA-DA bioink was 3D printed in grids with six layers with dimensions of 15 mm $\times$ 15 mm. Distance of 2.50 mm were used between the printed lines and alternative layers were printed at 90° angle. Printing pressure of 1.0 bar and speed of 6.0 mm s^{-1} was used. The samples were imaged immediately after printing and after seven days submerged in PBS at 37 °C. The thickness of the printed hydrogel filaments and pore geometry was quantified with Image J image processing and analysis software ($n = 6$). For each printed sample and time point, the filament thickness of six adjacent layers was evaluated from nine different filaments. Three randomly selected pores in each printed sample were included in image analysis. Pr was counted according to the following equation, where L means perimeter of the pore and A the pore area,

$$\mathrm{Pr} = \frac{L^2}{16A}.$$

2.7. Degradation study of the printed HA-DA bioink

To study the degradation and swelling characteristics of the printed structures, three parallel printed samples were subjected to neutral pH conditions. Briefly, cylindrical 3D structures ($\varnothing = 12$ mm) were printed with HA-DA bioink with 13 printed layers. The initial weight of the hydrogels was recorded. The gels were then submerged in 3 ml of PBS with pH 7.4. To observe swelling and subsequent degradation characteristics of the gels, the gels were re-weighed, placed in the incubator (37 °C), and the buffer was replaced daily for the first four days and subsequently every alternate day until 14 d. At each timepoint, the buffer was removed carefully, and the gels placed on the slides were dried to remove excess buffer that might introduce errors in the calculations. The remaining weight percentage was calculated by using the formula:

$$\text{Remaining weight } \% = \frac{\text{Measured weight}}{\text{Initial Weight}} \times 100.$$

2.8. Operational stability of printed HA-DA bioink

To characterize the mechanical stability of the 3D bioprinted structures of HA-DA bioink immersed in PBS, we performed rheology using a TA instruments' DHR-II rheometer at different timepoints for the printed structures. The oscillatory frequency sweep consisted of varying frequency of the deforming force, between 0.1 and 10 Hz with a constant strain value of 1% as determined from the amplitude sweep was performed to compare the stability by measuring the change in storage modulus of the HA-DA bioink immersed in PBS for 6 h, 24 h, 96 h, 168 h and 336 h. During this period, the storage modulus value at 1 Hz frequency was compared between gels of different timepoints to evaluate the operational stability of the printed constructs. All the measurements were performed with triplicates ($n = 3$).

2.9. Transparency analysis

The optical properties of the HA-DA bioink were analyzed by measuring its refractive index and transmittance. The refractive index was determined with surface plasmon resonance (SPR) equipment Navi™ 210A (BioNavis, Tampere, Finland). SPR Navi™ LayerSolver™ software was used to calculate the refractive index at wavelength 670 nm from the measured SPR curves. All pre-cleaned golden multi-parametric (MP)-SPR sensors were measured in air to acquire the backgrounds. Calibration of the SPR equipment was done separately for each gold sensor. Thereafter, the bioink samples (80 μl) were prepared onto the sensors and allowed to crosslink for 1 h in humid environment before measurements. The refractive index was measured from two points from each sample ($n = 4$). The optical transparency of the HA-DA bioink was further evaluated by measuring the transmittance with a spectrophotometer (Lamda 35 UV/VIS Spectrophotometer, Perkin Elmer) at the visible wavelength range (400–700 nm). The bioink samples ($n = 2$) were prepared into 1.6 ml semi-micro cuvettes (light path 10 mm, Sarstedt), centrifuged (1000 $\times$ g, 1 min) to remove air bubbles and allowed to crosslink in humid environment. The transmittance was measured after 1 h and 2 h of crosslinking. An empty cuvette (air) was used as a blank.

2.10. Self-healing and compression tests

The self-healing property of the HA-DA bioink was validated qualitatively with gel block fusion test and quantitatively with mechanical compression test. For these the bioink was prepared into two syringes. Red food dye with concentration of 4.2 μl ml^{-1} was mixed to the HA-DA bioink in the other syringe. The colorless and dyed bioinks were crosslinked in syringes for 24 h and cut into disc-shaped pieces. The pieces were cut into halves with a scalpel, and the cut surfaces of colorless and dyed bioink discs were positioned in tight contact and placed in a closed, humid environment. The self-healing was evaluated after 24 h visually and by lifting and pulling the structures with tweezers. The evaluation of the macroscopic self-healing properties was based on the ability of the bioink to maintain its structure under gravity and pulling force. Additionally, self-healing capacity was evaluated with a compression test utilizing a DHR-II Hybrid rheometer (TA Instruments). Bioink discs after 24 h of self-healing time (24 h self-healing, $n = 3$) was inserted between 12 mm parallel-plate geometry and exposed to an axial force with a displacement rate of 1.00 mm min^{-1}. A force curve was recorded and plotted against compression percentage. Same measurements were conducted to uncut bionink discs (control, $n = 3$) and bioink discs cut in half prior to measurements (0 h self-healing, $n = 3$). In this study, compressive modulus was calculated for the HA-DA bioink discs, since the cornea faces significant intraocular pressure in its native environment. The compression modulus was calculated using the following formula:

$$\text{Strain} : \varepsilon = \frac{\Delta L}{L},$$

where L is original sample length and ΔL is the change in length.

$$\text{Compressive modulus} = \frac{\sigma}{\varepsilon},$$

where σ is the compression stress.

2.11. Cells

hASCs were isolated mechanically and enzymatically from subcutaneous adipose tissue samples according to previously published protocols [35]. The isolated hASCs were characterized for their surface marker expression by flowcytometry (FACSAria; BD Biosciences, Erembodegem, Belgium) as shown previously [5]. Thereafter, hASCs were cultured in a medium containing DMEM/F-12 (Gibco™) supplemented with 5% human serum (type AB male, HIV tested from BioWest, Nuaillé, France), 1% GlutaMAX™ Supplement (Gibco™) and 1% penicillin/streptomycin (Gibco™) (hASC proliferation medium). Human ASCs were passaged upon confluency using TrypLE™ (Gibco™) and used for printing at passages 4–5. For printing, hASCs were enzymatically detached with TrypLE™, centrifuged and resuspended in culture medium for counting. Thereafter, hASCs were centrifuged, supernatant was removed, and the cells were resuspended in culture medium and mixed in HA-DA bioink with a cell density of 1.1×10^6 cells ml^{-1}.

Human ASCs have been previously shown to differentiate toward corneal stromal keratocytes (CSKs) *in vitro* [36, 37] and *in vivo* [38]. Here, we differentiated hASCs toward CSKs for seven days before using them for printing. For differentiation, hASCs were plated with cell density of 7000 cells cm^{-2} in a medium containing Advanced DMEM (Gibco™), 1% GlutaMAX™, 1% penicillin/streptomycin supplemented with 10 ng ml^{-1} basic fibroblast growth factor (PeproTech, London, United Kingdom), 0.1 mM ascorbic acid-2-phosphate (Sigma-Aldrich, United States) and 1 μM retinoic acid (Sigma-Aldrich) (CSK differentiation medium). For printing, hASC-CSKs were prepared as described above for hASCs. To further validate the differentiation protocol for hASC-CSKs, we plated hASCs on Costar® 24-well TC-treated well plate wells (Corning Incorporated) with cell seeding densities of 4500 and 7000 cells cm^{-2} and cultured the cells in CSK differentiation medium up to 28 d in 2D cultures. Fresh CSK differentiation medium was changed three times a week. Primary human cornea stromal keratocytes (hCSKs), isolated and cultured as previously described [4, 39], were used as controls.

Three printing strategies were explored in search of the most promising manufacturing strategy for 3D bioprinted corneal stroma. First, hASCs were printed and maintained in hASC proliferation medium after printing. Second, pre-printing differentiation approach was explored. Here, hASC-CSKs were differentiated for seven days before printing and maintained in the same CSK differentiation medium after printing. Third, post-printing differentiation approach was explored. Here, hASCs in hASCs proliferation medium were 3D bioprinted into cornea stroma mimicking structures, and differentiation toward CSKs was started after the printing process by placing the printed samples in CSK differentiation medium. Same cell density was used in all approaches and all the 3D printed cornea stromal structures were cultured *in vitro* up to 21 d.

Differentiation of hPSCs into neurons has been previously shown [40]. Here, human embryonic stem cell line Regea 08/023 was used and hPSCs were predifferentiated into neuronal cells (maturation stage, day 32 in differentiation protocol), before printing. For printing, neurons were detached with StemPro Accutase (Thermo Fisher Scientific), centrifuged, resuspended in culture medium and mixed in HA-DA bioink with density of 10×10^6 cell ml^{-1}. After printing, Neurobasal medium supplemented with 0.5% N2 supplement, 0.5 mM GlutaMAX (all from

Thermo Fischer Scientific), 0.1% penicillin/streptomycin (Lonza), 20 ng ml^{-1} brain-derived neurotrophic factor (BDNF, R&D Systems, Minneapolis, United States), 10 ng ml^{-1} glial-derived neurotrophic factor (GDNF, R&D Systems) and 500 μM dibutyryl-cyclicAMP (db-cAMP, Sigma-Aldrich) was used. All cell cultures were maintained at 37 °C in a 5% CO_2 atmosphere and 95% humidity.

For assessing the cytocompatibility of the HA-DA bioink, cell containing bioinks were printed into 2D structures, where ten parallel lines were printed with two overlapping layers. Falcon®35 mm TC-treated cell culture dishes (Corning®) were used as printing substrates in all studies. The distance between lines was set at 1 mm. For hASCs and hASC-CSKs printing pressure was set at 1.0 bar and printing speed of 6.0 mm s^{-1} was used. For hPSC-neurons, printing parameters of 0.9 bar and 9.0 mm s^{-1} were chosen. The printed 2D line structures were allowed to stabilize in 37 °C for 15 min before merging the structures to culture medium. For printing cornea stroma equivalents, 3D structures with ten layers were printed. Line distance of 400 μm was used. Each layer was printed at 90° angle to the previous layer. A stabilization period of 1 h in 37 °C was used for the 3D cornea stromal equivalents.

2.12. 3D bioprinted human cornea stroma with innervation

hPSC-neurons were added to the periphery of the printed cornea stroma equivalents to establish a proof-of-concept of 3D bioprinted cornea stroma with innervation. For this, hPSC-neurons were printed to periphery of the cylindrical stroma structure administrated as a hollow cylinder ($\varnothing = 12$ mm) surrounding the printed cornea stromal equivalent. Here, two experimental groups were explored: (a) cornea stromal structure without cells as control group and (b) cornea stromal structure with pre-differentiated hASC-CSKs as target cells for the neurons. The printing pressure and speed for each bioink were: 0.9 bar and 11.9 mm s^{-1} for HA-DA bioink containing hPSC-neurons, 1.5 bar and 6.8 mm s^{-1} for blank HA-DA bioink, and 0.9 bar and 10.5 mm s^{-1} for HA-DA bioink containing hASC-CSKs respectively.

2.13. Cytocompatibility

Cell viability in HA-DA bioink was evaluated for all investigated cell types with LIVE/DEAD® Viability/Cytotoxicity Kit for mammalian cells (Thermo Fischer Scientific) according to the manufacturer instructions. The viability of hASCs, hASC-CSKs and hPSC-neurons determined after one and seven days of printing from samples printed in line pattern. Furthermore, cell viability for 3D stromal mimicking structures with hASCs and hASC-CSKs was verified at the same time points and methods as described for line pattern.

PrestoBlue™ viability assay (Thermo Fischer Scientific) was performed at days 1, 3 and 7 for hASCs and hASC-CSKs printed in line patterns and in 3D stromal mimicking structures. The manufacturer's instructions were followed in detail for the analysis. For hASCs and hASC-CSKs printed in line patterns three to seven printed samples were analyzed in all three time points. For 3D bioprinted stromal equivalents with hASCs and hASC-CSKs four printed samples were included in cell proliferation analysis at each time point.

2.14. Indirect immunofluorescence (IF) staining

The cell morphology, proliferation, expression of cornea stroma specific markers and tissue formation after 3D bioprinting were investigated with IF stainings after 1, 3 and 7 days of printing. For hASCs and hASC-CSKs printed in line patterns, previously described protocol was followed [41]. Primary antibodies rabbit anti-Ki67 1:200 (Millipore) and goat anti-lumican 1:200 (R&D Systems) were used. As secondary antibodies, Alexa-Fluor conjugated 488 donkey anti-rabbit IgG and 647 donkey anti-goat IgG (both from Molecular Probes, Life Technologies) were used. Phalloidin-Tetramethylrhodamine B isothiocyanate (Sigma-Aldrich) was used for staining the cellular cytoskeleton and actin filaments of the printed cells and ProLong™ Gold Antifade Mountant with 4′,6-diamidino-2-phenylindole (DAPI) (Invitrogen™) was used for staining the nuclei. To evaluate the effectiveness of the differentiation protocol in 2D, primary antibodies including mouse anti-collagen I 1:100 (Abcam), rabbit anti-collagen V 1:100 (Millipore), goat anti-vimentin 1:200 (Millipore), mouse anti-α-smooth muscle actin (α-SMA) 1:400 (R&D), rabbit anti-aldehyde dehydrogenase 3A1 (ALDH3A1) 1:200 (Abcam), mouse anti-keratan sulfate (KS) 1:50 (Santa Cruz, Texas, United States) and rabbit-anti keratocan 1:100 (Santa Cruz) were explored. As secondary antibodies, Alexa-Fluor conjugated 488 donkey anti-rabbit IgG, 488 donkey anti-goat IgG and 568 donkey anti-mouse IgG in 1:400 dilution (all from Molecular Probes, Oregon, United States) were used.

3D bioprinted cornea stromal equivalents were fixed for IF after 14 and 21 d of printing with 4% paraformaldehyde (PFA) an washed thoroughly with PBS. Samples were blocked and permeabilized in PBS with 5% BSA and 0.2% Triton-X-100 overnight in RT. Primary antibodies goat anti-lumican 1:50, α-SMA 1:400, goat anti-vimentin 1:200, rabbit anti-connexin 43 1:50 (Abcam) were used. Primary antibodies were diluted in the blocking solution over three nights. Thereafter, samples were washed in the blocking buffer for 48 h. Used secondary antibodies are described above. The secondary ab solutions were prepared in the blocking buffer and incubated for 48 h in RT. Nuclei were counterstained with Hoechst 33342 (Invitrogen by Life technologies). Thereafter, thorough washing with PBS was done for 48 h. Finally,

the samples covered with VECTASHIELD® Antifade Mounting Medium (Vector Laboratories, California, United States). The samples were kept in +4 °C at least over night before imaging.

IF staining of hPSC-neurons printed in two-layered lines was performed after 1 and 7 days of printing by following previously published protocol for 2D [42]. Printed 3D stromal equivalents with innervation were analyzed after 7, 14 and 21 d of printing following previously established protocol [43] with minor modifications. Primary antibodies for hPSC-neurons in two-layered lines included mouse anti-βIII-tubulin (βIII-tub) 1:1000 (Sigma-Aldrich), rabbit anti-microtubule-associated protein 2 1:400 (MAP2, Merck) and rabbit anti-Ki67 1:400 (Millipore). Mouse anti-neurofilament heavy chain 1:500 (NFH, Sigma-Aldrich) was chosen as a primary antibody for neuronal extension visualization in 3D bioprinted cornea stromal equivalents. Secondary antibodies conjugated with Alexa Fluor 488 or 568 and washes with DAPI (2D samples), or Hoechst 33342 (3D samples) were used, followed by mounting with Vectashield (Vector Laboratories). Alexa Fluor™ 647 Phalloidin (Thermo Fischer Scientific) was incubated with secondary antibodies to visualize cytoskeleton of the hASC-CSKs.

IF stainings were visualized with Olympus IX 51 Fluorescence microscope (Olympus, Tokyo, Japan) and with LSM 800 confocal microscope (Carl Zeiss, Jena, Germany). Images were edited using ZEN Black Edition (Carl Zeiss Microscopy GmbH), Image J and Corel PHOTO-PAINT™ software (Corel corporation).

2.15. Hematoxylin and eosin (HE) staining

HE staining was carried out for cryosections from the 3D bioprinted stromal mimicking structures after 21 d of printing and human donor corneas were used as a control. HE staining was carried out following standard procedures and observed under a Nikon Eclipse TE200S microscope (Nikon Instruments Europe B.V., Amstelveen, Netherlands).

2.16. Gene expression analysis

Differences in relative expression level of lumican gene (LUM) and vimentin gene (VIM) were studied further with quantitative real-time polymerase chain reaction PCR (qPCR) as described previously with small modifications [44]. Total RNA was extracted from 3D printed stromal structures after 14 d of culture using TRI reagent (Sigma-Aldrich). RNA was purified from endogenous DNA using Dnase I (Thermo Fisher Scientific, Waltham, MA, USA). hCSKs from human corneas and undifferentiated hASCs in 2D cultures were used as a control for qPCR. Samples were collected from two individual experiments. Three printed samples were studied for each sample condition in both experiments ($n = 6$). TaqMan® Gene Expression Assays (Applied Biosystems Inc, Massachusetts, United States) were used for PCR reaction: LUMICAN (HS00929860_m1), VIMENTIN (Hs00958111_m1) and GAPDH (Hs99999905_m1). The results were analyzed using 7300 System SDS Software (Applied Biosystems Inc.). $2-\Delta\Delta$Ct method [45] was used for the relative quantification of LUM and VIM. The values for each sample were normalized to expression levels of GAPDH. The expression level of undifferentiated hASCs in 2D cultures was set as the calibrator (fold change equals 1).

2.17. Porcine cornea organ culture

The corneal organ culture using excised porcine corneas was conducted as previously described [5, 24] with slight modifications. Briefly, fresh porcine eyes were stripped of excess tissue and disinfected with 2% povidone iodine (Betadine®, Leiras, Helsinki, Finland), and the corneas were dissected from the eyes in aseptic conditions. The corneas were cultured partially submerged in Advanced DMEM supplemented with 1% GlutaMAX™, 1% Penicillin-Streptomycin and 0.25 μg ml^{-1} amphotericin B (Thermo Fisher Scientific) at +37 °C in 5% CO_2 for two days prior to implantation of the 3D bioprinted stromal mimicking constructs printed with hASC-CSKs. hASC-CSKs containing 3D stromal mimicking structures were cultured for seven days before implantation. Implantation was performed on a Barron artificial anterior chamber (Katena products Inc., Denville, NJ, USA), to allow handling of the cornea during the operation. A 5 mm trephine (Robbins Instruments, Chatham, NJ, USA) was used to make a partial thickness cut to the center of the cornea. The stromal tissue was removed from the trephined area using a crescent knife (Bauch&Lomb Inc., Rochester, NY, USA). The trephine was also used to punch out a 5 mm diameter piece from the 3D printed stromal construct, then placed into the stromal wound bed. After implantation, the corneas were moved from the artificial anterior chamber back into culture plates and cultured partially submerged in hASC-CSK medium for 21 d at +37 °C in 5% CO_2. For analysis, the corneal organ cultures were fixed in 4% PFA for 4 h at RT, rinsed with PBS and incubated in 20% sucrose solution overnight at +4 °C. Thereafter, the samples were embedded in Tissue-Tek OCT (Science Services, Munich, Germany), snap frozen at liquid nitrogen and stored in −80 °C. For IF and HE staining, cryosections of 10 μm were prepared and air dried for 1 h at RT. The cryosections were IF stained as described above. Mouse anti-human cytoplasm STEM121 1:80 (Takara Bio Inc., Japan) was used to detect hASC-CSKs in porcine cornea organ cultures.

2.18. Statistical analysis

The statistical significance of shape fidelity analysis, PrestoBlue™ cell proliferation as well as qPCR data was determined with non-parametric

Mann–Whitney U test. P-values $\leqslant 0.05$ were considered statistically significant. The statistical data analysis was carried out with IBM SPSS Statistics software.

2.19. Ethical issues

This study was carried out under approvals from the local ethics committee of the Pirkanmaa hospital district Finland that allow to extract and use hASCs for research purposes (R15161), to use human donor corneas unsuitable for transplantation for research purposes (R11134) and to use hPSCs in neuronal research (R20159). New cell lines were not derived for this study.

3. Results

3.1. Developed HA-DA bioink demonstrates excellent printability and shape fidelity

The degree of dopamine functionalization on HA-DA was determined to be 4.5 mol% with respect to the disaccharide repeat units of hyaluronan using a best-fit line drawn through the linear portion of the standard curve by UV–vis spectrophotometric method. Similarly, the ^{1}H-NMR analysis (supplementary figure 1(a)) indicated the degree of modification to be 5 mol% by calculating the ratio of the *N*-acetyl peak of HA at 1.96 ppm and the aromatic protons of dopamine between 6.7 and 7.5 ppm for HA-DA. Further the dopamine conjugation on HA was ascertained by analyzing the ATR-FTIR spectra of free DA, HA and HA-DA in (supplementary figure 2). The DA showed the following characteristic peaks consistent with the literatures: 3345 cm^{-1} (amine N–H stretching), 3039 cm^{-1} (aromatic O–H stretching), 2946 cm^{-1} (alkyl C–H stretching), 1614 cm^{-1} (amine N–H bending), 1493 cm^{-1} (aromatic C = C stretching) and several peaks in the 650–1300 cm^{-1} region due to the aliphatic chains [46]. Both the HA, and HA-DA showed broad peaks at 3100–3600 cm^{-1} due to the stretching vibrations of –OH groups, and amine N–H groups. We also observed the peaks around 1033–1152 cm^{-1} due to the C–O–C hemiacetal saccharide units in the hyaluronan backbone. The asymmetric stretching vibrations of carboxylate around 1375–1405 cm^{-1}, the symmetrical stretching vibrations of $–CH_2$ group around 2895 cm^{-1}, the amide I and II the bands around 1550–1561 cm^{-1} were also present in both HA and HA-DA. In the case of HA-DA, the distinctive –C = O and amide stretching appears at 1645 cm^{-1} and 1733 cm^{-1} due to conjugation of DA on carboxyl group of HA [47]. The hydrazide modifications on HA-CDH and HA-DA-CDH were optimized to be 10–12 mol% with respect to the repeated disaccharide units of HA as determined by TNBS assay. The aldehyde modification on HA was determined to be 11 mol% by ^{1}H-NMR analysis (supplementary figure 1(b)) by integrating the ratio of the *N*-acetyl peak of HA at 1.96 ppm and t-butyl carbazate methyl peaks at 1.22 ppm.

The printability of HA-based bioinks was first assessed by measuring the viscosity of both HA and HA-DA bioinks. The viscosity value was less than 100 Pa for HA bioink which indicates high fluidity (figure 1(a)). In contrast, HA-DA bioink showed initial mounting shear rate with measured viscosity values of over 2000 Pa. As the shear rate was increased, the HA-DA bioink showed increased shear thinning behavior, confirming its injectability without clogging in the nozzle during printing. To understand the robustness of the bioinks, we performed further shear-thinning experiments under the application of periodic low (0.01 s^{-1}) and high shear rate (10 s^{-1}). Here, HA-DA bioink exhibited excellent shear-thinning ability within the performed seven cycles (figure 1(b)). Interestingly, the HA-bioink crumpled into pieces on the rheometer plate after four cycles (figure 1(c)). Thereafter, we evaluated the elasticity of the bioinks by measuring the storage and loss modulus under periodic low and high strain. The HA-DA bioink (figure 1(d)) showed higher storage modulus under the application of 1% strain on the first cycle compared to the HA bioink (figure 1(e)). Although the shear strain was increased periodically, the HA-DA bioink showed excellent modulus recovery, exhibiting its efficacy as a shear-thinning and self-healing composition.

The printability of the HA-based bioinks was evaluated by printing two-layered grids. The HA bioink did not form filaments upon printing (figure 1(f)) and behaved fluid-like and failed to maintain the printed grid structure during the printing process. In contrast, the HA-DA bioink displayed excellent filament formation with both investigated printing parameters resulting in uniform filaments and a clear grid structure. Here, a 90 min biofabrication window was obtained for the HA-DA bioink for printing. Subsequently, we analyzed the shape fidelity of HA-DA bioink further by printing six layered lattice structures. Immediately after printing the lattice line thickness of 334 $\pm$ 58 μm was measured (figure 1(g)). Only slight increase up to 363 $\pm$ 77 μm was seen during seven days in culture. Pr of 0.95 $\pm$ 0.04 was obtained immediately after printing and it decreased only slightly after seven days of culture down to 0.92 $\pm$ 0.02 (figure 1(h)). After seven days of culture, the printed lattice structures were uniform with clear visible grid structure and open pores (figure 1(i)).

The structural stability of the printed 3D HA-DA cylinders was also measured. The swelling property of the printed construct (figure 1(l)) immersed in phosphate buffered saline (PBS, pH 7.4) was analyzed by calculating the change in weight % over 14 d (figure 1(k)). Interestingly, we observed swelling within 3 h of the immersion of the printed constructs

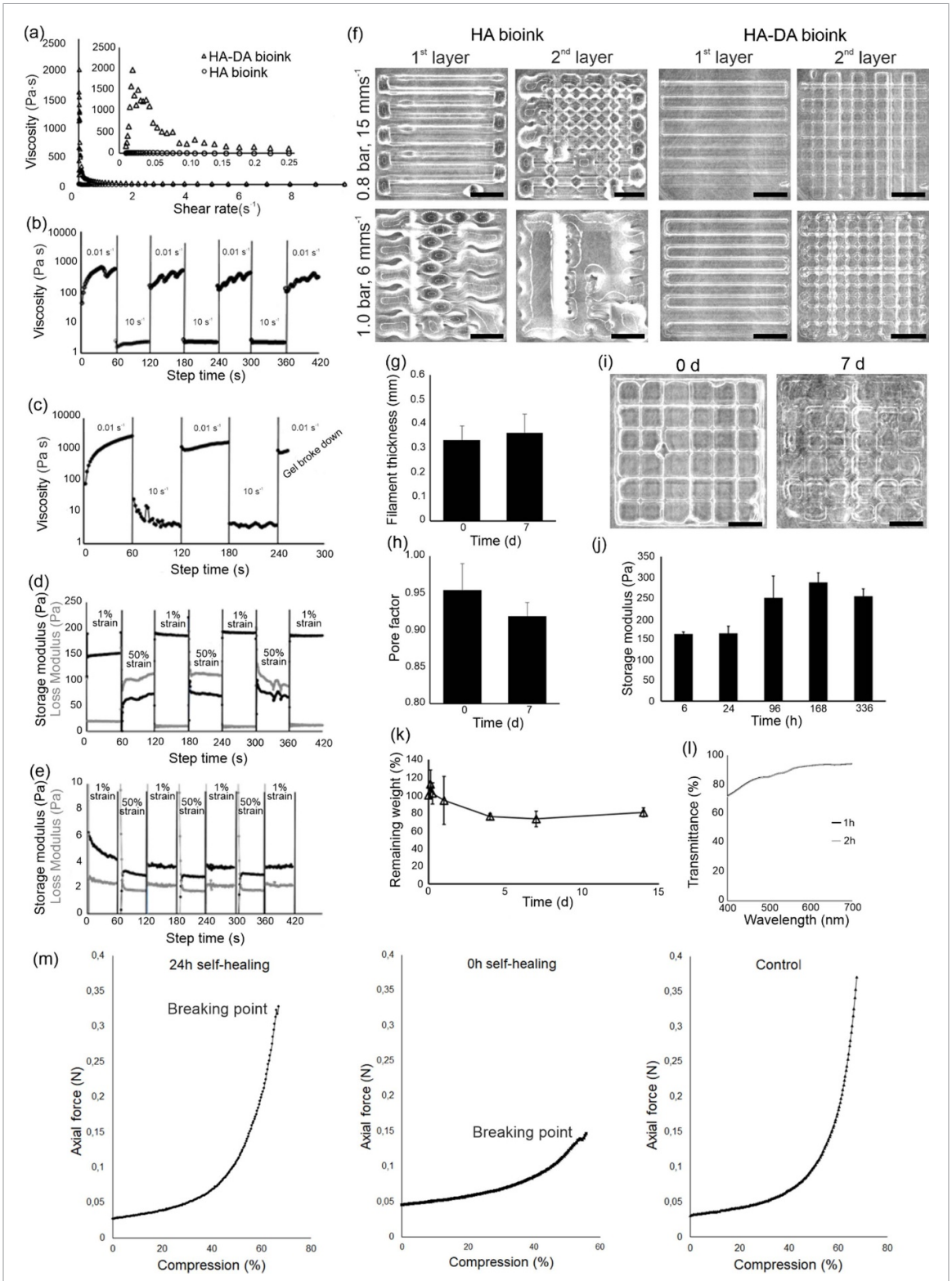

Figure 1. The HA-DA bioink shows high resolution printing with excellent shape fidelity and self-healing properties. (a) Shear thinning of HA-DA and HA bioink under continuous flow. The shear thinning of (b) HA-DA and (c) HA bioink under cyclic strain. (c) Strain recovery of the fully crosslinked (d) HA-DA bioink and (e) HA bioink. (f) Printability of HA and HA-DA bioinks with two different printing parameters. Scale bars 5 mm. Shape fidelity of the printed HA-DA bioink structures evaluated with (g) filament thickness and (h) pore factor. (i) Images of printed lattices after the printing and seven days in culture. Scale bars 5 mm. (j) Storage modulus of the 3D bioprinted structures indicating structural stability in culture. (k) Degradation and swelling behavior of the printed structures upon time. (l) Transmittance of the HA-DA bioink. (m) HA-DA bioink shows tissue self-healing properties in quantitative mechanical compression test.

into PBS, then a slight weight loss until day 4. Thereafter, no further weight loss until day 14 was detected. The free HA and collagen added to the bioink formulation, although improved the printability of the ink, might have caused this anomalous observation within early timepoints. We also observed a

slight reduction of the storage modulus of the gels immersed in PBS on day 1 (24 h, 188 ± 34 Pa) compared to storage modulus of the gels at 6 h (164 ± 17 Pa) (figure 1(j)). The reduction of the amount of materials in the printed constructs payed a predominant role in early timepoints. Upto day 7, the gradual auto-oxidation of dopamine moiety at pH 7.4 resulted in a slight increase in storage modulus which was evidence from the transparent color change in to slight yellow. The storage modulus at 336 h remained higher compared to 6 h, further emphasizing the important role of dopamine in maintaining the structural stability of the constructs.

The transmittance of the HA-DA bioink was measured after 1 and 2 h of crosslinking to analyze transparency (figure 1(l)). After 1 h, the transmittance of HA-DA bioink was 71.9 ± 1.3% at 400 nm and 94.1 ± 1.5% at 700 nm. After 2 h, transmittance was 71.6 ± 1.0% at 400 nm and 94.3 ± 1.5% at 700 nm. Refractive index of the HA-DA bioink was measured at 1.343 ± 0.000 52 after 1 h of crosslinking.

We also assessed the self-healing properties of the HA-DA bioinks after one day (figure 1(m)). After 24 h of self-healing, the reassembled hydrogel discs were cohesively bound to each other (supplementary figure 3(a)). The control HA-DA hydrogel discs withstood high compression and recovered perfectly after compressive load was removed. The reassembled hydrogel discs broke ideally from the cut seam (supplementary figure 3(b)) and breaking point of the reassembled hydrogel discs was also observed in the force curves. Sample with 0 h of self-healing was notably weaker than other samples and significantly lower axial force (0.14 ± 0.041 N, $n = 3$) as well as lower compression percentage (54.0 ± 1.3%, $n = 3$) at the breaking point compared to 24 h self-healing and control discs. On the contrary, force curves of control and 24 h of self-healing hydrogel discs were very similar and breaking of 24 h self-healing discs occurred with a high compression percentage (66.0 ± 1.33%, $n = 3$) and higher axial force (0.32 ± 0.066 N, $n = 3$) than with 0 h self-healing discs, indicating self-healing capacity of the hydrogels. Compressive modulus for the HA-DA bioink was 10.3 kPa after 24 h of crosslinking.

3.2. Cytocompatibility of HA-DA bioink with hASCs and hASC-CSKs

To explore the cytocompatibility of the HA-DA bioink, we 3D bioprinted hASCs and hASC-CSKs into two layered lines and 3D cornea stromal equivalents. Thereafter, we evaluated the viability of the cells after one and seven days of printing. High cell viability of >95% was detected with both cell types in printed lines with hardly any dead cells (figure 2(a)). The number of dead cells did not increase upon culture. High cell viability was also detected in printed 3D stromal structures. There, hASCs survived the printing process slightly better compared to hASC-CSKs (figure 2(a)), where the number of dead cells increased a bit upon culture in 3D cornea stroma. Despite, majority of the printed cells were viable after seven days of printing. Cytocompatibility was further confirmed by IF staining and PrestoBlue^{TM} analysis. IF staining of the printed lines with phalloidin revealed elongated cell morphology of both cell types already after 1 day (figure 2(b)). A clear increase in cell number was detected with hASCs until day 7 during which they remained aligned according to the original printing pattern. Number of hASC-CSKs increased slightly between day 1 and 3. However, no evident cell proliferation was demonstrated thereafter for hASC-CSKs. Both cell types showed positive expression of proliferation marker Ki67 after printing. Printing of both cells resulted in patterned cell structures and organization. PrestoBlue^{TM} analysis confirmed proliferation of the printed cells in HA-DA bioink (figures 2(c) and (d)). hASCs showed significantly higher cell proliferation in both two layered lines and 3D stromal structures at day 7 compared to day 1 and 3 ($p < 0.001$). With hASC-CSKs, an increase in proliferation was seen from day 1–3 in two layered lines ($p < 0.001$), whereas a drop in proliferation was detected in 3D stromal structures at day 3. The cell proliferation between day 3 and 7 was on similar level in two layered lines for hASC-CSKs. In 3D stromal structures, slight increase in proliferation was seen with hASC-CSKs when comparing day 7 against day 1, but it was not statistically significant. These results are in line with previous findings with hASCs, where decreased cell proliferation capacity was detected upon differentiation toward osteogenic lineage [48]. In addition, hASC-CSKs demonstrated strong expression of lumican (figure 2(e)). To further evaluate tissue formation in the printed stromal structures, we carried out confocal imaging for the 3D stromal structures after 14 d of printing. Positive staining against gap junction protein connexin 43 (Cx43) was detected for both cell types indicating formation of cell–cell interactions in the printed structures (figure 2(f)). Elongated cell morphology and cellular networks were also seen in 3D confocal images for both cell types (figures 2(g)–(h)).

3.3. 3D bioprinting of cornea stroma mimicking structures using HA-DA bioink

Next, we explored three different printing strategies for TE of cornea stroma and explored the resemblance of the printed constructs upon culture. In first approach, undifferentiated hASCs were printed and maintained in their proliferation medium also after bioprinting. In pre-printing approach, hASCs were differentiated toward CSKs before printing. In post-printing approach, differentiation of hASCs toward CSKs was commenced after printing by placing the printed structures in CSK differentiation medium. Here, the 3D bioprinted structures utilizing all three printing strategies demonstrated that hASCs and

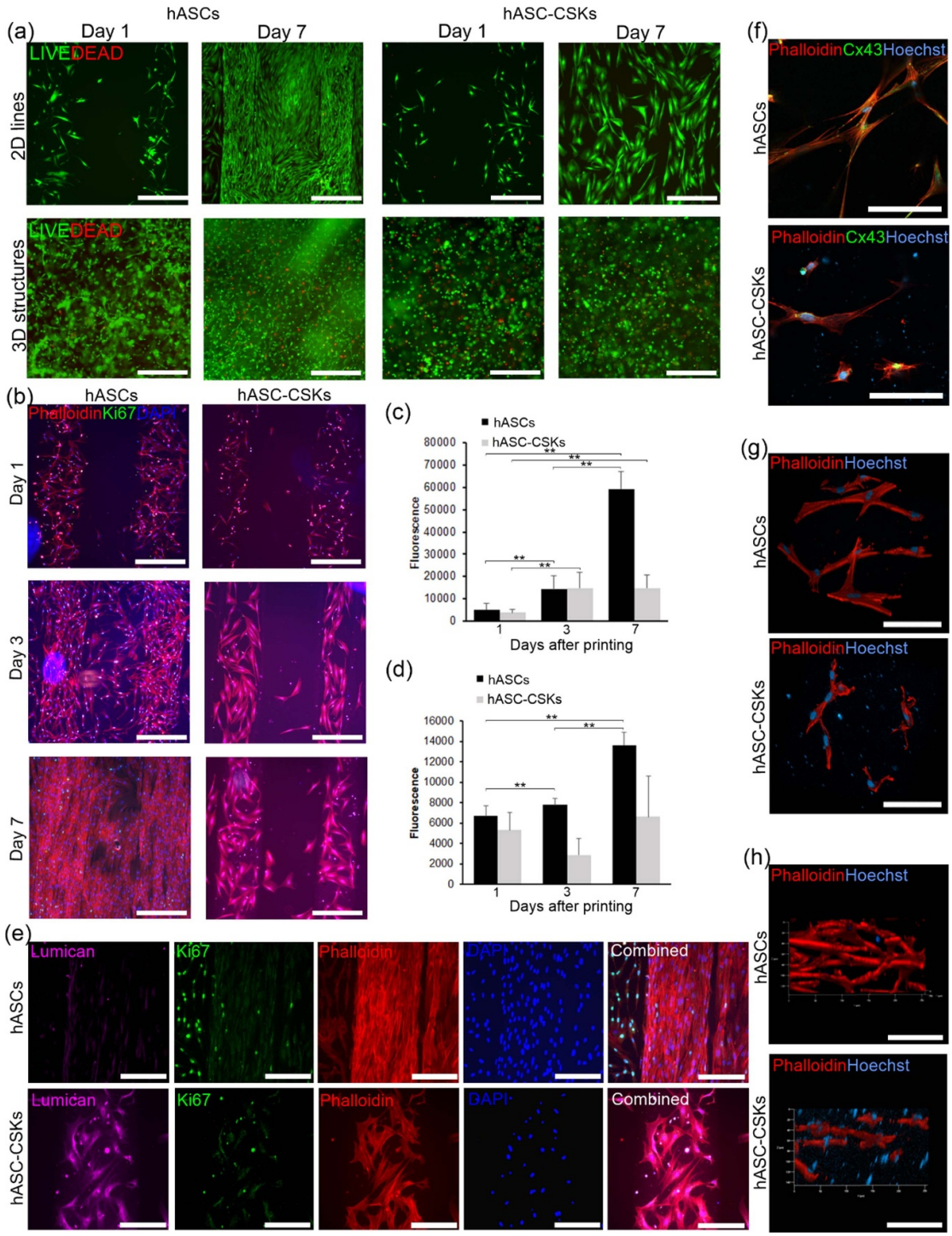

Figure 2. Cytocompatibility of HA-DA bioink with hASCs and hASC-CSKs. (a) Viability of cells printed as lines and 3D structures after the following and 7 days of printing (live cells = green, dead cells = red). (b) Cell migration (phalloidin = red) and proliferating cells (Ki67 = green) of hASCs and hASC-CSKs in printed lines at one, three and seven days after printing. Scale bars 500 μm. Cell proliferation of hASCs and hASC-CSKs in printed in lines (c) and 3D structures (d) after 1, 3 and 7 days of printing analyzed with PrestoBlue^{TM} ($^{**} = p < 0.001$). (e) Cell morphology, proliferation and cornea stroma marker expression in printed lines after 7 days of printing. Proliferating cells were stained against Ki67 (green), cell morphology was visualized with phalloidin (red) and cornea stroma marker expression detected with lumican (purple). Scale bars 200 μm. (f) Confocal images of the cell–cell interactions in 3D bioprinted stroma after 14 d since printing. Cellular cytoskeleton visualized with phalloidin (red) and cell–cell interaction with gap junction protein Cx43 (green). (g) 3D rotated confocal images of cells in 3D structures after 14 d of printing. (h) Side view of 3D bioprinted structures from 3D rotated confocal images. Scale bars 100 μm ((f)–(h)) nuclei are visualized with DAPI and Hoechst 33342 (blue).

hASC-CSKs were organized sparsely throughout the 3D structure when examining the cross-sections with HE stainings (figures 3(a) and (b)). hASCs showed elongated cell morphology throughout the printed structure. Similar organization was detected with pre-printing differentiating hASC-CSKs. In contrast, far less elongations were seen in the cross-sections of post-printing differentiated hASC-CSKs (figures 3(a)

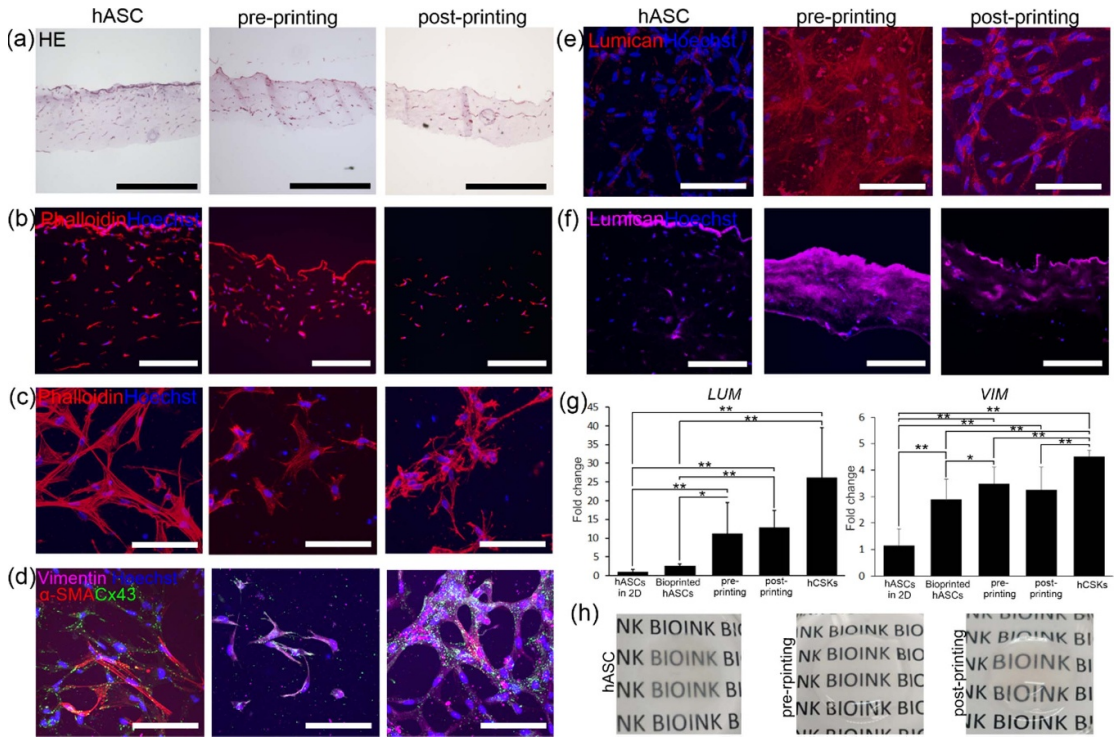

Figure 3. 3D bioprinting strategies for human cornea stroma structures. (a) HE stainings from cryosections after 21 d of printing for hASCs, pre-printing differentiated hASC-CSKs and post-printing hASC-CSKs where differentiation of cells was initiated after 3D bioprinting process. Scale bars 500 μm. (b) Cell distribution, morphology and orientation in 3D bioprinted structures visualized with phalloidin (red) from cryosections after 21 d of printing. Scale bars 200 μm. Confocal maximum intensity projection images of the cells in 3D bioprinted stroma 14 d after printing visualized with phalloidin (red) (c) confocal maximum intensity projection images of vimentin (purple), Cx43 (green) and α-SMA (red) (d), and lumican (red) (e) after 21 d of printing. Scale bars 100 μm (d), (e). (f) Lumican (purple) expression visualized from cryosections after 21 d of printing. Scale bars 200 μm. (g) qPCR analysis of LUM and VIM ($^{*} = p < 0.05$, $^{**} = p < 0.001$). hCSKs were used as a control. Transparency of the 3D bioprinted corneal stroma structures after 14 d in culture (h). Nuclei are visualized with Hoeschst 33342 (blue).

and (b)). Initial organization of the printed cells into lamellar structures was seen with all approaches. Considerable differences were seen in cell morphology upon culture between the different printing strategies (figure 3(c)). hASCs showed elongated cell morphology with dense cellular networks in the printed structures. The hASC-CSKs in both pre-and post-printing approaches showed more dendritic cell morphology with roundish cell bodies and thin cellular extensions. All the printing strategies resulted in formation of cell–cell interactions detected with positive staining against Cx43 (figure 3(d)). The number of cell–cell interactions was higher with hASCs and post-printing hASC-CSKs.

Vimentin is a major structural intermediate filament protein expressed in low levels in normal CSKs [49]. Here low expression of vimentin was detected with hASC-CSKs in both pre-and post-printing approaches in IF staining (figure 3(d)), whereas expression was absent in hASCs. In qPCR analysis, all bioprinted samples showed increased expression of VIM compared to the undifferentiated hASCs in 2D cultures (figure 3(g)) ($p < 0.001$). Increased VIM expression was detected with hASC-CSKs in pre-printing approach compared to 3D bioprinted hASCs ($p < 0.05$). On the contrary, hASCs showed positive expression of α-SMA in IF staining, whereas little or no expression α-SMA was seen in hASC-CSKs in both pre- and post-printing approaches. Lumican is a member of the small leucine-rich proteoglycan family, and a major KS proteoglycan found in corneal stroma [50]. The highest lumican expression was detected in printed structures prepared with hASC-CSKs in pre-printing strategy shown here by confocal maximum intensity projection images (figure 3(e)) and IF staining of histological sections (figure 3(f)) with fibrillar organization and density. In addition, low positive staining was detected in printed structures with post-printing strategy with intracellular and granular expression pattern (figure 3(e)). In qPCR analysis, both pre-printing and post-printing approaches showed increased LUM expression compared to undifferentiated hASCs in 2D ($p < 0.001$) and 3D printed hASCs ($p < 0.01$) (figure 3(g)). However, the expression of both LUM and VIM was lower in hASC-CSKs compared to the hCSKs used as a positive control ($p < 0.001$). This data suggests that the two printing strategies have resulted in structures where differentiation of hASCs toward the cornea keratocyte lineage has been induced. To validate the effectiveness of the pre-printing protocol toward CSK lineage, we carried out more detailed characterization of the cells in 2D cultures with IF. There, positive expression of cornea stroma specific

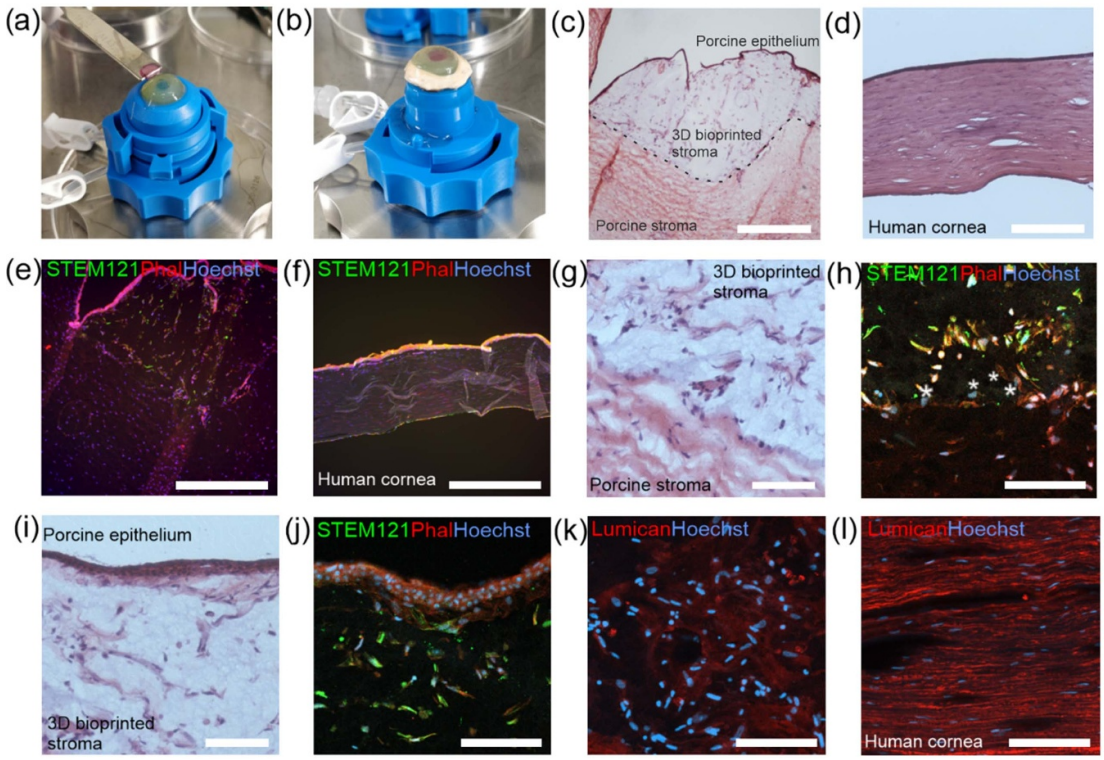

Figure 4. 3D bioprinted stromal structures in porcine organotypic cultures after 21 d of culture. Implantation of 3D bioprinted structures to the porcine corneas in a Barron artificial anterior chamber (a) porcine cornea with 3D bioprinted stromal mimicking structure after implantation (b) HE staining of organotypic cultures with 3D bioprinted cornea stroma mimicking structure (indicated with dashed line) (c) central human corneal stroma (d) Scale bars 200 μm ((c), (d)). (e) Integration of the 3D bioprinted stroma into host tissue visualized from cryosections with human cell specific marker STEM121 (green) and phalloidin (red). (f) The human corneal stroma is shown as a control. Scale bars 500 μm ((e), (f)). (g) High-magnification images of the interface between 3D bioprinted structure and the porcine stroma from HE and (h) IF stainings at the basal side of the implant. Cells that were negative for STEM121 (green) were seen in the printed structure (market with white *) indicating integration of host cells to the printed stromal structure. High-magnification images of the apical side 3D bioprinted structure from (i) HE and (j) IF stainings. (k) 3D bioprinted structures in organotypic cultures showed expression of cornea stroma marker Lumican (red). (l) Human cornea was used as a control. Scale bars 100 μm ((g)–(l)) Nuclei are visualized with Hoechst 33342 (blue).

markers ALDH3A1, Col V, vimentin, and keratocan was detected (supplementary figure 4) in both hASC-CSKs and hCSKs used as a control.

While inspecting the transparency illustrated by photography (figure 3(h)) of the printed structures after 14 d of printing, some opacity of the printed structures with hASCs was detected. In contrast, samples printed with pre-and post-printing differentiation approaches showed transparent structures.

3.4. Integration of 3D bioprinted corneal stromal structures to host tissue

Having explored the 3D bioprinting of human cornea stroma with HA-DA bioink we next assessed the performance of the printed cornea stromal constructs upon implantation in an *ex vivo* cornea organ culture model. Pre-printing differentiation strategy was chosen based on the results in previous experiments. We performed an anterior lamellar keratoplasty procedure for excised porcine corneas (figures 4(a) and (b)) and transplanted the 3D bioprinted cornea stroma onto the wound site. The integration of the printed structure to the host cornea was evaluated after 21 d in culture with HE and IF staining from cryocross-sections. The implanted 3D bioprinted cornea stromal structures maintained in place during the culture period without additional means of securing the implant in place or with the help of stromal pocket approach. After 21 d, the 3D bioprinted cornea stromal structures showed excellent attachment and adhesion to the host cornea (figure 4(c)). Human cornea was used as a control (figure 4(d)). IF staining showed the STEM121 positive cells in the printed structure indicating the presence of human cells in the porcine *ex vivo* model (figure 4(e)) and control human cornea (figure 4(f)). High magnification images (figure 4(g)) demonstrated that the printed structure is tightly attached to the underlying host stroma. Moreover, cells that were negative for STEM121 were seen inside the printed structure when inspecting the interface of the implanted structure and host cornea (figure 4(h)) indicating migration of porcine cells to the printed structure. Additionally, on the apical side, host porcine epithelium had grown over the 3D bioprinted cornea structure (figure 4(i)). Stratified porcine cornea epithelium covered the STEM121 positive human cell containing printed stromal structures

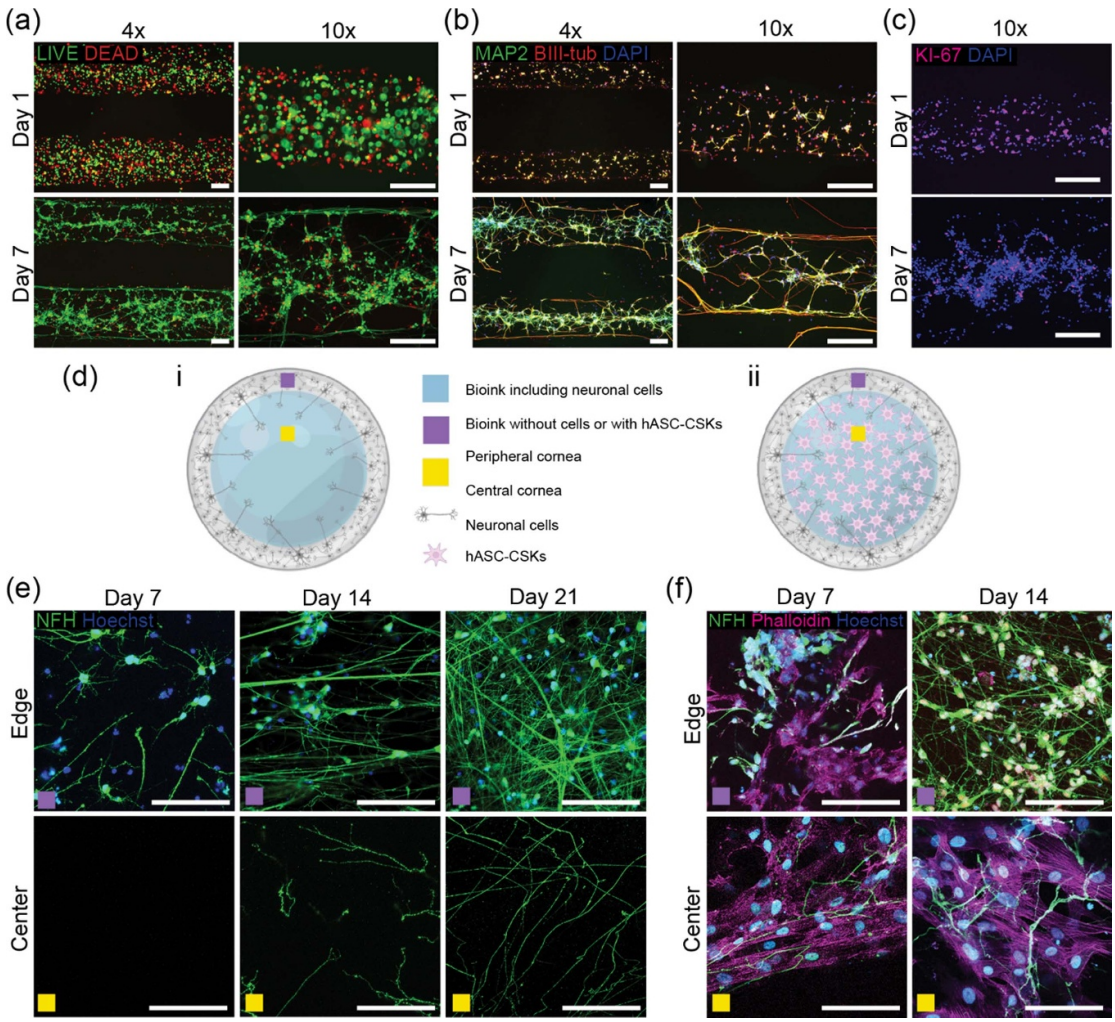

Figure 5. Innervated 3D bioprinted cornea stromal equivalent. (a) Viability of the neuronal cells in bioink printed in lines after one and seven days of printing (live cells = green, dead cells = red). (b) Expression of neuronal markers βIII-tub (red) and MAP2 (green) of cells in printed lines after 1 and 7 days of printing. (c) Positive staining of proliferation marker Ki67 (magenta) in printed lines after 1 and 7 days of printing. (d). Schematic illustration of innervated experimental groups: 3D bioprinted cornea stroma equivalent in which neuronal cells are bioprinted to the periphery of the cornea (position highlighted with purple square). Target at the central cornea is (i) bioink without cells (control) or (ii) bioink including hASC-CSKs (position highlighted in yellow square). Illustration created with Biorender.com. Development of innervation over the time in 3D control group (e) and with hASC-CSKs as target cells at the center (f) morphology of the neurons is stained with NFH (green) and hASC-CSKs with phalloidin (magenta). Scale bars are 100 μm.

(figure 4(j)). Finally, slight expression of lumican was detected also in printed structure in *ex vivo* cultures (figure 4(k)) although the expression was moderate compared to lumican expression seen in native human cornea (figure 4(l)).

3.5. 3D bioprinting cornea stroma mimicking tissue with innervation

The cytocompatibility of hPSC-neurons with HA-DA bioink was investigated with LIVE/DEAD analysis. The neurons showed good viability. The majority of the cells were viable after 1 day of printing and the number of dead cells decreased after 7 days of printing when observed visually (figure 5(a)). Neuronal phenotype was addressed with expression of neuronal markers βIII-tub and MAP2. The neurons showed short neurite growth already after 1 day of printing, and after 7 days of printing clear neuronal network with long axons following the printed line pattern was formed (figure 5(b)). Number of proliferating (Ki67 positive) cells was detected in both time points, but the number of positive cells was decreased after 7 days (figure 5(c)). Taken together, these findings indicate good cytocompatibility of the HA-DA bioink with hPSC-derived neuronal cells.

The innervation into 3D bioprinted stromal equivalents was successfully added by printing the neuronal cells to the periphery of the structure (figure 5(d)). The development of innervation into the printed stromal equivalents temporally was studied for control group without target cells (figure 5(d)i) or printed structures with hASC-CSKs as target cells (figure 5(d)ii). The samples without target cells were cultured for 21 d and the samples with hASC-CSKs as target cells for 14 d. In both groups long neurite growth toward the central cornea was

detected over time (figures 5(e) and (f)). However, the innervation seemed to develop faster and earlier in the samples with hASC-CSKs as target cells. There, the long axons expressing NFH can be seen at the central part of the 3D cornea structure among hASC-CSKs already after 7 d, whereas in the control group axons cannot be seen in bioink without the target cells until 14 d of culture. Similar axonal growth was reach in the control group only after 21 d of culture. In the co-culture group axons growing among and between the hASC-CSKs seemed to form bundles of several axons after 14 d of printing (figure 5(f)).

4. Discussion

Bioinks are materials that contain a single or multi component matrix components with a living cells or growth factors that are loaded into 3D bioprinters to produce native tissue-like constructs [51]. A few requirements have been set for bioinks to perform well in 3D bioprinting, including good printability and shape fidelity, sufficient structural stability, biocompatibility and effective biological performance. Traditional bioinks have been compromising printability for cytocompatibility, whereas the next generation of bioinks should aim to overcome these concessions by offering optimal performance with both features [10]. Importantly, physical printing process is only a short window in the lifespan of a printed constructs and system must support and facilitate tissue formation after it is printed [52]. Making tissue constructs with the desired functional and biomechanical properties from available biomaterials remains a challenge also in 3D bioprinting of corneal tissues [53].

Previously, cornea stroma mimicking structures have been printed using bioinks comprising of methacrylated gelatin [6], sodium alginate and gelatin [54], methacrylated collagen and sodium alginate [4], corneal stroma-derived decellularized extracellular matrix [8], light-activated decellularized extracellular matrix bioinks with ruthenium/sodium persulfate [55], collagen type I and agarose [56], blends of human collagen type I with human plasma and thrombin [5] and a bovine cornea-derived decellularized extracellular matrix [57]. Here, we tackle the challenges in cornea TE by developing a next generation bioink for 3D bioprinting of cornea stromal equivalents. Clinically suitable and biodegradable HA was chosen as a base of the bioink. To increase tissue adhesive property, dopamine was covalently grafted to the polymer backbone, and dynamic hydrazone crosslinking was used for stabilizing the printed structures. To our knowledge, this is the first study to exploit HA-based bioinks with dynamic covalent chemistry for 3D bioprinting of cornea.

Viscosity is the resistance of a fluid to flow under the application of stress and has a great influence on both the print fidelity and efficiency of cell encapsulation [3]. In this study, we explored the viscosity profiles of the developed bioinks as a function of shear strain. The HA bioink resulted in low viscosity and a fluid-like behavior. Moreover, a lack of filament formation and shape retention was witnessed in 3D printing, indicating that the hydrazone crosslinked HA bioink is not suitable for 3D bioprinting with low concentrations. The covalent grafting of dopamine moieties to the polymer backbone was necessary to obtain bioink composition with high viscosity, good printability and shape fidelity. The viscosity measurements of the HA-DA bioink indicated secondary interactions mediated by the dopamine moiety which induced physical associations like H-bonding, and ionic interactions with collagen present in the formulation [58]. Since the developed bioinks are based on pre-crosslinking before printing, it was very important to assess the mechanical stability of the bioinks under dynamic loading. Generally, the pre-crosslinking approach imparts higher extrusion force during printing which further results in impaired printed structures. The HA-DA bioink (figure 1(d)) showed higher storage modulus under the application of 1% strain on the first cycle compared to the HA bioink (figure 1(e)), which further proved the important role of dopamine in stabilizing the printed structure. Dynamic hydrazone crosslinking chemistry together with dopamine mediated secondary interactions thus provided excellent structural stability to the HA-DA bioink compared to the HA-bioink as evidenced from the rheological measurements. In mechanical compression test, the HA-DA bioink withstood high compression forces and recovered perfectly after removal of the compressive load. Compressive modulus of 10.3 kPa was measured for cell-free HA-DA bioinks in this study. In a previous study, compressive modulus of the 3D printed GelMA structures for cornea stroma was 10 kPa after one day of printing [59]. Thus, HA-DA bioink shows comparative mechanical properties to the photocrosslinkable hydrogels used in 3D bioprinting of cornea. Moreover, HA-DA bioink demonstrated self-healing properties.

Previously, blends of tissue adhesive gallol-functionalized HA and gelatin have been explored as bioink for extrusion printing [60]. There, the gallol-modification of extra cellular matrix (ECM) components allowed shear-thinning properties by dynamic hydrogen bonds on short timescales. However, only short-term stability of six days in culture was reported. In other study, catechol-modified HA bioink was combined with alginate for increased printability of the covalent cross-linking hydrogels [61]. Crosslinking of thiolated Pluronic F-127 with dopamine-conjugated gelatin and dopamine conjugated HA resulted in thermoresponsive bioinks for neural and glial applications [62]. Structural stability for this bioink

was reached either with photopolymerization of methacrylated gelatin functionalized with dopamine or by metal complexation of dopamine conjugated gelatin using ferric nitrate. Unlike the many bioinks that are subjected to photo- or ionic-crosslinking after passing the nozzle to maintain the fidelity of the printed structures, the developed hydrazone crosslinked HA-DA bioink does not require any post-processing steps to gain sufficient stability upon culture. This is highly advantageous that promote simplified printing process when upscaling the manufacturing process of 3D bioprinted corneal stroma equivalents.

The printing resolution in extrusion printing is one the drawbacks of the technology resulting in poor tissue mimicry. It is mainly dictated by the bioink properties and the nozzle diameter. The combination of high pressure and small needle diameter exposes cells to considerable shear stress, which can lead to cell damage and death [63]. In extrusion printing, the resolution is typically limited in the range of hundred micrometers to millimeters, as shear stress at the dispenser tip, which inversely correlates with the nozzle diameter, should be minimized to prevent decrease in cellular viability [52]. In this study, we used 32 G straight needles with inner diameter of 100 μm for printing of living cells. Even though relatively high printing pressure of 1.0 bar was used, we obtained high cell viability and proliferation with hASCs and hASC-CSKs. Previously, hydrazone crosslinked HA gels have been printed with nozzle diameters of 18–25 G [25]. However, in that study, the forces needed for bioink extrusion with 23 G and 25 G needles were found directly to affect negatively on cell viability. In previous studies of cornea TE, conical nozzles with inner diameter ranging from 150 to 300 μm had been used with extrusion printing [4, 56]. Here, the HA-DA bioink with excellent shear thinning properties upon the biofabrication window resulted in high-resolution printing with micro-extrusion. Previously, the use of straight nozzles has been shown to significantly decrease cell viability compared to conical nozzles in gelatin methacrylamide bioinks [64, 65]. In our study, printing with the straight and long nozzles resulted in good cell viability and tissue formation after printing, indicating that the developed HA-DA bioink shielded cells from mechanical stresses during extrusion printing. In a previous study by Kim *et al*, extrusion printing with 30 G nozzle diameter resulted in increased collagen fibril alignment and expression of corneal stromal cell markers with human turbinate-derived mesenchymal stem cell derived CSKs in decellularized cornea extracellular matrix based bioink [8]. However, the use of 30 G nozzle resulted in significant expression of α-SMA and 25 G nozzles were used in their further experiments due to this. α-SMA expression represents a phenotypic characteristic of myofibroblasts, which has been shown to contribute to the loss of corneal transparency [66]. In the present study, low expression of α-SMA was seen with printed hASC-CSKs in 3D bioprinted cornea stromal structures using 32 G nozzle. Thus, the developed HA-DA bioink provides means to challenge the technological limitations of extrusion bioprinting in achievable resolution. Moreover, the combination of excellent printability and cytocompatibility indicates that the developed HA-DA bioink has immense potential as a next generation bioink for corneal TE.

To date, CSKs have been mainly preferred as a cell source for 3D bioprinting of cornea stroma [4, 67]. However, expanding CSKs *in vitro* is challenging and there is a huge shortage of cornea donor tissue limiting their use in corneal TE and cell therapy [68, 69]. Human mesenchymal stem cells such as hASCs have proven to be capable of producing new ECM proteins within the host cornea stroma, modulate pre-existing scars and enhance transparency by corneal stroma remodeling [70]. Moreover, *in vitro* [36] and *in vivo* [38] differentiation of hASCs toward CSKs has been previously reported and in recent clinical trials moderate improvements in visual acuity were seen, highlighting the potential of hASCs in cornea TE applications [70]. Previously, the regeneration of cornea stromal mimicking structures with hASCs has been shown using human collagen I based bioink in laser-assisted 3D bioprinting [5]. There, a cornea stroma mimicking structure with adequate cell organization was achieved. Nevertheless, an additional supporting membrane was needed for sufficient mechanical stability for handling of the printed structures. Human turbinate-derived mesenchymal stem cell derived CSKs have been also explored as an alternative cell source for 3D bioprinting of cornea stroma [57]. To the best of our knowledge, the present study is the first to show 3D bioprinted cornea stroma with hASC-CSKs relevant for clinical applications [71].

In the present study, we explored three different printing strategies for manufacturing corneal stromal equivalents using hASCs as a cellular component. All three approaches resulted in adequate cell organization and cell–cell interaction formation. Both pre- and post-printing differentiation approaches resulted in cellular characteristics typical for CSKs found in the native cornea [72]. The future success of corneal 3D bioprinting will ultimately depend on the ability of printed cells to mediate ECM remodeling in order to establish tissue functionality [4]. In this study, the highest expression of lumican, a member of the small leucine-rich proteoglycan family with reported expression in cornea [50], as well as transparency was found in cornea stromal equivalents 3D bioprinted with pre-printing approach. Instead, cornea stroma equivalents 3D bioprinted with hASCs resulted in slight opacity. This could be caused by the high cell proliferation of the hASCs after printing (figure 2(d)) in 3D structures. This is in line with a previous study by Sorkio *et al*, where 3D bioprinted cornea stromal

structures with hASCs showed slight opacity upon culture [5]. It should be noted that brown coloration is a distinct feature of dopamine-containing materials due to self-polymerization of the dopamine residues [73], but it is not seen here with the developed HA-DA bioink upon 14 d of culture. The human cornea has high transparency for light transmission. The corneal light-transmittance rises, from 80% at 380 nm over 90% between 500 and 1300 nm [74, 75]. Here, the developed bioink showed transmittance values close to the values reported for the native cornea.

When addressing different printing strategies for cornea TE, other aspects besides tissue mimicry should be considered when choosing a printing strategy, including challenges and opportunities in the standardization of the production process [53]. Notably, purification of the cell population would not be possible in post-printing differentiation, leaving little control on the composition of the construct along maturation after printing. In addition, during post-printing differentiation, human stem cells have been shown result in the partial or total loss of the original printed pattern [76]. Thus, pre-printing differentiation approach holds several advantages over other proposed printing strategies, such as better control on the cells that will be included in the construct [77]. Yet, it should be noted that special attention needs to be addressed in the future on achieving more efficient differentiation protocols of hASCs toward CSK lineage as well as the phenotype and maturation stage of the cells need to be more thoroughly characterized for optimal performance and microenvironment of the printed structures.

To explore the integration of the 3D bioprinted cornea stromal equivalents, they were implanted into *ex vivo* porcine corneas with pre-differentiation approach. After 21 d of implantation, without any additional means of fixing the implant on stromal wound, the printed cornea stromal equivalents were well integrated to the host porcine tissue with stratified porcine cornea epithelium fully covering the implanted structure. Moreover, cells that were not positive for human cell marker STEM-121 were seen inside the implanted structure, meaning potential migration of the host porcine stromal cells into the printed structure. Host cell migration and stromal adhesion in *ex vivo* models have been previously reported to be suggestive of tissue biocompatibility of the bioengineered corneas [78]. Importantly, the printed stromal equivalents withstood surgical handling without any additional supportive membranes, which is a promising improvement from the previous work with 3D bioprinted corneal stromal mimicking structures using hASCs [5]. However, the tissue biocompatibility of 3D bioprinted corneal stromal equivalents should be validated in *in vivo* setting in the future to fully explore the suitability of this approach for cornea TE.

Finally, restoring proper axonal integration of implanted TE grafts with the host system are goals in dire need of attention and action [79]. The axonal ingrowth and elongation are supported by environmental cues such as ECM components and bioactive molecules. The developed HA-DA bioink contains components, HA and collagen, found in native neuronal tissues [80] offering favorable microenvironment for the printed neurons. Here, LIVE/DEAD and IF data indicated excellent cytocompatibility of the HA-DA bioink with hPSC-neurons. Moreover, dopamine is well known neurotransmitter improving neurite outgrowth [81]. Previously, dopamine has been shown to promote neural network growth in gelatin methacrylate bionk [82] as well as HA-based 3D hydrogels [58]. Here, we demonstrated the successful ingrowth of neuronal extensions into the 3D bioprinted cornea stromal equivalents. Previously, the innervation has been shown to improve viability of the 3D *in vitro* corneal models using animal derived neurons [28, 83] and human-derived neurons [84, 85]. *In vivo,* corneal cells secrete bioactive molecules such as nerve growth factor inducing axonal chemotaxis [83]. The innervation developed to the 3D bioprinted cornea stromal equivalents gradually in structures with and without target cells in the stroma. The hASC-CSKs as target cells attracted axons to the stroma faster, and long axons were detected among the hASC-CSKs already after 7 d of culture. In contrast, without target cells neurite growth was detected only after 14 d culture. This 3D bioprinted innervated 3D cornea model holds great potential not only for cornea TE purposes, but also as platform for drug screening and disease modeling.

5. Conclusions

We have developed a HA-based bioink using dynamic covalent chemistry that fills the demands of next generation bioinks with excellent printability, stability, cytocompatibility as well as efficient tissue formation after printing without using photo-crosslinking. Moreover, the HA-DA bioink showed good mechanical and self-healing properties. Here, we demonstrated the feasibility of the developed bioink for 3D bioprinting of human cornea stroma equivalents using clinically potential human stem cells. These 3D bioprinted cornea stroma equivalents showed excellent integration to host tissue in *ex vivo* cultures. Moreover, we manufactured the first 3D bioprinted cornea tissue model with innervation. The developed bioink and the printed human stem cell derived cornea stromal equivalents hold great potential for various future cornea TE applications.

Data availability statement

The data generated and/or analyzed during the current study are not publicly available for legal/ethical reasons but are available from the corresponding author on reasonable request.

Acknowledgments

Tampere University Imaging and CellTech Cores are thanked for providing assistance and equipment for the study. The authors wish to thank Outi Melin, Hanna Pekkanen and Hanna Mäkelä for technical assistance. The Cell and Tissue Bank Regea (Tampere University) is also acknowledged for their assistance in providing cadaveric donor corneas for research purposes.

Author's contributions

A M had the lead role in designing and performing the experiments, analyzing and interpreting the data, acquiring funding and writing the manuscript. S S designed and performed the experiments, analyzed and interpreted the data and drafted the manuscript. L H designed and performed the experiments, analyzed and interpreted the data and drafted the manuscript. V R conceived and designed the experiments and interpreted the data. P P conceived and designed the experiments and interpreted the data. M K conceived and designed the experiments and interpreted the data. S N contributed regents/materials/analysis tools and participated in the critical revision of the manuscript; S M contributed materials/reagents tools and participated in the critical revision of the manuscript. O O designed the experiments, interpreted the data and participated in the critical revision of the manuscript and final approval of the article. H S acquired funding, designed the experiments, interpreted the data; participated in the critical revision of the manuscript and final approval of the article.

Conflict of interest

Mörö and Oommen are inventors of a pending patent application related to the bioink innovation reported in this study. Based on the Act on the Right in Inventions made at Higher Education Institutions in Finland, all authors employed by Tampere University have given all rights to the University and thus have declared no competing interests. Mörö and Skottman are co-founders and shareholders in StemSight Ltd without any connection to the technology and results reported in this manuscript. The other authors declare no conflicts of interests.

Funding

This study was supported by the Academy of Finland (324082 A M, 336665 S N, 336666 S M, 326588 S M, 312413 S M, 337607 S M), Jane and Aatos Erkko foundation (H S and A M), the Finnish Cultural Foundation, Instrumentarium Science Foundation, Anu Kirra Foundation, Juliana von Wendt Foundation, Orion Research Foundation, Björkqvist Foundation and European Union's Horizon 2020 Marie Sklodowska-Curie Grant Program (713645).

ORCID iD

Anni Mörö https://orcid.org/0000-0002-0301-4745

References

[1] Gain P, Jullienne R, He Z, Aldossary M, Acquart S, Cognasse F and Thuret G 2016 Global survey of corneal transplantation and eye banking *JAMA Ophthalmol.* **134** 167
[2] Alió Del Barrio J L, Arnalich-Montiel F, De Miguel M P, El Zarif M and Alió J L 2021 Corneal stroma regeneration: preclinical studies *Exp. Eye Res.* **202** 108314
[3] Schwab A, Levato R, D'Este M, Piluso S, Eglin D and Malda J 2020 Printability and shape fidelity of bioinks in 3D bioprinting *Chem. Rev.* **120** 11028–55
[4] Isaacson A, Swioklo S and Connon C J 2018 3D bioprinting of a corneal stroma equivalent *Exp. Eye Res.* **173** 188–93
[5] Sorkio A, Koch L, Koivusalo L, Deiwick A, Miettinen S, Chichkov B and Skottman H 2018 Human stem cell based corneal tissue mimicking structures using laser-assisted 3D bioprinting and functional bioinks *Biomaterials* **171** 57–71
[6] Mahdavi S S, Abdekhodaie M J, Kumar H, Mashayekhan S, Baradaran-Rafii A and Kim K 2020 Stereolithography 3D bioprinting method for fabrication of human corneal stroma equivalent *Ann. Biomed. Eng.* **48** 1955–70
[7] Zhang B *et al* 2019 Integrated 3D bioprinting-based geometry-control strategy for fabricating corneal substitutes *J. Zhejiang Univ. Sci.* B **20** 945–59
[8] Kim H, Jang J, Park J, Lee K-P, Lee S, Lee D-M, Kim K H, Kim H K and Cho D-W 2019 Shear-induced alignment of collagen fibrils using 3D cell printing for corneal stroma tissue engineering *Biofabrication* **11** 035017
[9] Gomez-Florit M, Pardo A, Domingues R M A, Graça A L, Babo P S, Reis R L and Gomes M E 2020 Natural-based hydrogels for tissue engineering applications *Molecules* **25** 5858
[10] Decante G, Costa J B, Silva-Correia J, Collins M N, Reis R L and Oliveira J M 2021 Engineering bioinks for 3D bioprinting *Biofabrication* **13** 032001
[11] Hintze V, Schnabelrauch M and Rother S 2022 Chemical modification of hyaluronan and their biomedical applications *Front. Chem.* **10** 830671
[12] Jorgensen A M, Yoo J J and Atala A 2020 Solid organ bioprinting: strategies to achieve organ function *Chem. Rev.* **120** 11093–127
[13] Skardal A *et al* 2015 A hydrogel bioink toolkit for mimicking native tissue biochemical and mechanical properties in bioprinted tissue constructs *Acta Biomater.* **25** 24–34
[14] Spearman B S, Agrawal N K, Rubiano A, Simmons C S, Mobini S and Schmidt C E 2020 Tunable methacrylated hyaluronic acid-based hydrogels as scaffolds for soft tissue engineering applications *J. Biomed. Mater. Res.* A **108** 279–91
[15] Poldervaart M T, Goversen B, De Ruijter M, Abbadessa A, Melchels F P W, Öner F C, Dhert W J A, Vermonden T and

Alblas J 2017 3D bioprinting of methacrylated hyaluronic acid (MeHA) hydrogel with intrinsic osteogenicity *PLoS One* **12** e0177628
[16] Wang R, Deng S, Wu Y, Wei H, Jing G, Zhang B, Liu F, Tian H, Chen X and Tian W 2022 Remodelling 3D printed GelMA-HA corneal scaffolds by cornea stromal cells *Colloid Interface Sci. Commun.* **49** 100632
[17] Knowlton S, Yenilmez B, Anand S and Tasoglu S 2017 Photocrosslinking-based bioprinting: examining crosslinking schemes *Bioprinting* **5** 10–18
[18] Zhao D, Tie C, Cheng B, Yang S, Wang X, Sun Z, Yin M, Zhu H and Yin M 2020 Effect of altering photocrosslinking conditions on the physical properties of alginate gels and the survival of photoencapsulated cells *Polym. Degrad. Stab.* **179** 109297
[19] Gopinathan J and Noh I 2018 Click chemistry-based injectable hydrogels and bioprinting inks for tissue engineering applications *Tissue Eng. Regen. Med.* **15** 531–46
[20] Zou Y, Zhang L, Yang L, Zhu F, Ding M, Lin F, Wang Z and Li Y 2018 "Click" chemistry in polymeric scaffolds: bioactive materials for tissue engineering *J. Control. Release* **273** 160–79
[21] Mueller E, Poulin I, Bodnaryk W J and Hoare T 2022 Click chemistry hydrogels for extrusion bioprinting: progress, challenges, and opportunities *Biomacromolecules* **23** 619–40
[22] Jiang Y, Chen J, Deng C, Suuronen E J and Zhong Z 2014 Click hydrogels, microgels and nanogels: emerging platforms for drug delivery and tissue engineering *Biomaterials* **35** 4969–85
[23] Koivusalo L, Karvinen J, Sorsa E, Jönkkäri I, Väliaho J, Kallio P, Ilmarinen T, Miettinen S, Skottman H and Kellomäki M 2018 Hydrazone crosslinked hyaluronan-based hydrogels for therapeutic delivery of adipose stem cells to treat corneal defects *Mater. Sci. Eng.* C **85** 68–78
[24] Koivusalo L, Kauppila M, Samanta S, Parihar V S, Ilmarinen T, Miettinen S, Oommen O P and Skottman H 2019 Tissue adhesive hyaluronic acid hydrogels for sutureless stem cell delivery and regeneration of corneal epithelium and stroma *Biomaterials* **225** 119516
[25] Wang L L, Highley C B, Yeh Y-C, Galarraga J H, Uman S and Burdick J A 2018 Three-dimensional extrusion bioprinting of single- and double-network hydrogels containing dynamic covalent crosslinks *J. Biomed. Mater. Res.* A **106** 865–75
[26] Das S, Gordián-Vélez W J, Ledebur H C, Mourkioti F, Rompolas P, Chen H I, Serruya M D and Cullen D K 2020 Innervation: the missing link for biofabricated tissues and organs *npj Regen. Med.* **5** 11
[27] Medeiros C S and Santhiago M R 2020 Corneal nerves anatomy, function, injury and regeneration *Exp. Eye Res.* **200** 108243
[28] Wang S, Ghezzi C E, Gomes R, Pollard R E, Funderburgh J L and Kaplan D L 2017 *In vitro* 3D corneal tissue model with epithelium, stroma, and innervation *Biomaterials* **112** 1–9
[29] Hirano M, Huang Y, Jarquin D V, De La Garza Hernández R L, Jodat Y A, Cerón E L, García-Rivera L E and Shin S R 2021 3D bioprinted human iPSC-derived somatosensory constructs with functional and highly purified sensory neuron networks *Biofabrication* **13** 035046
[30] Sharma R, Smits I P M, De La Vega L, Lee C and Willerth S M 2020 3D bioprinting pluripotent stem cell derived neural tissues using a novel fibrin bioink containing drug releasing microspheres *Front. Bioeng. Biotechnol.* **8** 57
[31] Abelseth E, Abelseth L, De La Vega L, Beyer S T, Wadsworth S J and Willerth S M 2019 3D printing of neural tissues derived from human induced pluripotent stem cells using a fibrin-based bioink *ACS Biomater. Sci. Eng.* **5** 234–43
[32] Salaris S, Colosi C, Brighi B, Soloperto S, de Turris T, Benedetti B, Ghirga G, Rosito R, Di Angelantonio S and Rosa R 2019 3D bioprinted human cortical neural constructs derived from induced pluripotent stem cells *J. Clin. Med.* **8** 1595
[33] Oommen O P, Wang S, Kisiel M, Sloff M, Hilborn J and Varghese O P 2013 Smart design of stable extracellular matrix mimetic hydrogel: synthesis, characterization, and *in vitro* and *in vivo* evaluation for tissue engineering *Adv. Funct. Mater.* **23** 1273–80
[34] Varghese O P, Wang S, Oommen O P and Yan H 2013 Mild and efficient strategy for site-selective aldehyde modification of glycosaminoglycans: tailoring hydrogels with tunable release of growth factor *Biomacromolecules* **14** 346–69
[35] Lindroos B, Boucher S, Chase L, Kuokkanen H, Huhtala H, Haataja R, Vemuri M, Suuronen R and Miettinen S 2009 Serum-free, xeno-free culture media maintain the proliferation rate and multipotentiality of adipose stem cells *in vitro Cytotherapy* **11** 958–72
[36] Kumar A, Xu Y, Yang E, Wang Y and Du Y 2019 Fidelity of long-term cryopreserved adipose-derived stem cells for differentiation into cells of ocular and other lineages *Exp. Eye Res.* **189** 107860
[37] Du Y, Roh D S, Funderburgh M L, Mann M M, Marra K G, Peter Rubin J, Li X and Funderburgh J L 2010 Adipose-derived stem cells differentiate to keratocytes *in vitro Mol. Vis.* **16** 2680–9
[38] Alio Del Barrio J L *et al* 2015 Acellular human corneal matrix sheets seeded with human adipose-derived mesenchymal stem cells integrate functionally in an experimental animal model *Exp. Eye Res.* **132** 91–100
[39] Foster J W, Gouveia R M and Connon C J 2015 Low-glucose enhances keratocyte-characteristic phenotype from corneal stromal cells in serum-free conditions *Sci. Rep.* **5** 10839
[40] Hyvärinen T, Hyysalo A, Kapucu F E, Aarnos L, Vinogradov A, Eglen S J, Ylä-Outinen L and Narkilahti S 2019 Functional characterization of human pluripotent stem cell-derived cortical networks differentiated on laminin-521 substrate: comparison to rat cortical cultures *Sci. Rep.* **9** 17125
[41] Sorkio A E, Vuorimaa-Laukkanen E P, Hakola H M, Liang H, Ujula T A, Valle-Delgado J J, Österberg M, Yliperttula M L and Skottman H 2015 Biomimetic collagen I and IV double layer Langmuir-Schaefer films asmicroenvironment for human pluripotent stem cell derived retinal pigment epithelial cells *Biomaterials* **51** 257–69
[42] Lappalainen R S, Salomäki M, Ylä-Outinen L, Heikkilä T J, Hyttinen J A, Pihlajamäki H, Suuronen R, Skottman H and Narkilahti S 2010 Similarly derived and cultured hESC lines show variation in their developmental potential towards neuronal cells in long-term culture *Regen. Med.* **5** 749–62
[43] Honkamäki L, Joki T, Grigoryev N A, Levon K, Ylä-Outinen L and Narkilahti S 2021 Novel method to produce a layered 3D scaffold for human pluripotent stem cell-derived neuronal cells *J. Neurosci. Methods* **350** 109043
[44] Sorkio A, Hongisto H, Kaarniranta K, Uusitalo H, Juuti-Uusitalo K and Skottman H 2014 Structure and barrier properties of human embryonic stem cell-derived retinal pigment epithelial cells are affected by extracellular matrix protein coating *Tissue Eng.* A **20** 622–34
[45] Schmittgen T D and Livak K J 2001 Analysis of relative gene expression data using real-time quantitative PCR and the 2(-delta delta C(T)) method *Methods* **25** 402–8
[46] Thakur A, Ranote S, Kumar D, Bhardwaj K K, Gupta R and Chauhan G S 2018 Synthesis of a PEGylated dopamine ester with enhanced antibacterial and antifungal activity *ACS Omega* **3** 7925–33
[47] Liu Y, Qiu Y, Ni S, Zhang X, Sun H, Song W and Li X 2020 Mussel-inspired biocoating for improving the adhesion of dental pulp stem cells in dental pulp regeneration *Macromol. Rapid Commun.* **41** 2000102
[48] Ojansivu M, Vanhatupa S, Björkvik L, Häkkänen H, Kellomäki M, Autio R, Ihalainen J A, Hupa L and Miettinen S 2015 Bioactive glass ions as strong enhancers of osteogenic differentiation in human adipose stem cells *Acta Biomater.* **21** 190–203
[49] Das S K, Gupta I, Cho Y K, Zhang X, Uehara H, Muddana S K, Bernhisel A A, Archer B and Ambati B K 2014

Vimentin knockdown decreases corneal opacity *Investig. Ophthalmol. Vis. Sci.* **55** 4030–40
[50] Carlson E C, Liu C-Y, Chikama T-I, Hayashi Y, Kao C W-C, Birk D E, Funderburgh J L, Jester J V and Kao W W-Y 2005 Keratocan, a cornea-specific keratan sulfate proteoglycan, is regulated by lumican *J. Biol. Chem.* **280** 25541–7
[51] Zhang J, Wehrle E, Rubert M and Müller R 2021 3D bioprinting of human tissues: biofabrication, bioinks and bioreactors *Int. J. Mol. Sci.* **22** 3971
[52] Willson K, Atala A and Yoo J J 2021 Bioprinting au natural: the biologics of bioinks *Biomolecules* **11** 1593
[53] Murphy S V, De Coppi P and Atala A 2020 Opportunities and challenges of translational 3D bioprinting *Nat. Biomed. Eng.* **4** 370–80
[54] Kutlehria S, Dinh T C, Bagde A, Patel N, Gebeyehu A and Singh M 2020 High-throughput 3D bioprinting of corneal stromal equivalents *J. Biomed. Mater. Res.* B **108** 2981–94
[55] Kim H, Kang B, Cui X, Lee S-H, Lee K, Cho D-W, Hwang W, Woodfield T B F, Lim K S and Jang J 2021 Light-activated decellularized extracellular matrix-based bioinks for volumetric tissue analogs at the centimeter scale *Adv. Funct. Mater.* **31** 2170231
[56] Duarte Campos D *et al* 2019 Bioprinting at the interface: 3D corneal substitutes bioprinted using human stromal keratocytes and collagen-based hydrogels *Biomed. Tech.* **64** 1945–53
[57] Kim H, Park M-N, Kim J, Jang J, Kim H-K and Cho D-W 2019 Characterization of cornea-specific bioink: high transparency, improved *in vivo* safety *J. Tissue Eng.* **10** 204173141882338
[58] Samanta S, Ylä-Outinen L, Rangasami V K, Narkilahti S and Oommen O P 2022 Bidirectional cell-matrix interaction dictates neuronal network formation in a brain-mimetic 3D scaffold *Acta Biomater.* **140** 314–23
[59] Kilic Bektas C and Hasirci V 2020 Cell loaded 3D bioprinted GelMA hydrogels for corneal stroma engineering *Biomater. Sci.* **8** 438–49
[60] Shin M, Galarraga J H, Kwon M Y, Lee H and Burdick J A 2019 Gallol-derived ECM-mimetic adhesive bioinks exhibiting temporal shear-thinning and stabilization behavior *Acta Biomater.* **95** 165–75
[61] Guo Z, Xia J, Mi S and Sun W 2020 Mussel-inspired naturally derived double-network hydrogels and their application in 3D printing: from soft, injectable bioadhesives to mechanically strong hydrogels *ACS Biomater. Sci. Eng.* **6** 1798–808
[62] Haring A P, Thompson E G, Tong Y, Laheri S, Cesewski E, Sontheimer H and Johnson B N 2019 Process- and bio-inspired hydrogels for 3D bioprinting of soft free-standing neural and glial tissues *Biofabrication* **11** 025009
[63] Fischer L *et al* 2022 Calcium supplementation of bioinks reduces shear stress-induced cell damage during bioprinting *Biofabrication* **14** 045005
[64] Billiet T, Gevaert E, De Schryver T, Cornelissen M and Dubruel P 2014 The 3D printing of gelatin methacrylamide cell-laden tissue-engineered constructs with high cell viability *Biomaterials* **35** 49–62
[65] Liu W *et al* 2017 Extrusion bioprinting of shear-thinning gelatin methacryloyl bioinks *Adv. Healthcare Mater.* **6** 1601451
[66] Torricelli A A M and Wilson S E 2014 Cellular and extracellular matrix modulation of corneal stromal opacity *Exp. Eye Res.* **129** 151–60
[67] Kilic Bektas C, Burcu A, Gedikoglu G, Telek H H, Ornek F and Hasirci V 2019 Methacrylated gelatin hydrogels as corneal stroma substitutes: *in vivo* study *J. Biomater. Sci. Polym. Ed.* **30** 1803–21
[68] Binte N Z, Yusoff M, Riau A K, Yam G H F, Halim N S H B and Mehta J S 2022 Isolation and propagation of human corneal stromal keratocytes for tissue engineering and cell therapy *Cells* **11** 178
[69] West-Mays J A and Dwivedi D J 2006 The keratocyte: corneal stromal cell with variable repair phenotypes *Int. J. Biochem. Cell Biol.* **38** 1625–31
[70] El Zarif M, Alió J L, Alió Del Barrio J L, Abdul Jawad K, Palazón-Bru A, Abdul Jawad Z, De Miguel M P and Makdissy N 2021 Corneal stromal regeneration therapy for advanced keratoconus: long-term outcomes at 3 years *Cornea* **40** 741–54
[71] Del Barrio J L *et al* 2022 Corneal regeneration using adipose-derived mesenchymal stem cells *Cells* **11** 2549
[72] Jester J V, Barry P A, Lind G J, Petroll W M, Garana R and Cavanagh H D 1994 Corneal keratocytes: *in situ* and *in vitro* organization of cytoskeletal contractile proteins *Investig. Ophthalmol. Vis. Sci.* **35** 730–43
[73] Shin J *et al* 2015 Tissue adhesive catechol-modified hyaluronic acid hydrogel for effective, minimally invasive cell therapy *Adv. Funct. Mater.* **25** 3814–24
[74] Fuest M, Yam G H F, Mehta J S and Campos D F D 2020 Prospects and challenges of translational corneal bioprinting *Bioengineering* **7** 71
[75] Meek K M and Knupp C 2015 Corneal structure and transparency *Prog. Retin. Eye Res.* **49** 1–16
[76] Koch L, Deiwick A, Franke A, Schwanke K, Haverich A, Zweigerdt R and Chichkov B 2018 Laser bioprinting of human induced pluripotent stem cells—the effect of printing and biomaterials on cell survival, pluripotency, and differentiation *Biofabrication* **10** 035005
[77] Salaris F and Rosa A 2019 Construction of 3D *in vitro* models by bioprinting human pluripotent stem cells: challenges and opportunities *Brain Res.* **1723** 146393
[78] Rafat M *et al* 2022 Bioengineered corneal tissue for minimally invasive vision restoration in advanced keratoconus in two clinical cohorts *Nat. Biotechnol.* (https://doi.org/10.1038/s41587-022-01408-w)
[79] Al-Aqaba M A, Dhillon V K, Mohammed I, Said D G and Dua H S 2019 Corneal nerves in health and disease *Prog. Retin. Eye Res.* **73** 100762
[80] Rutka J T, Apodaca G, Stern R and Rosenblum M 1988 The extracellular matrix of the central and peripheral nervous systems: structure and function *J. Neurosurg.* **69** 155–70
[81] Gao J, Kim Y M, Coe H, Zern B, Sheppard B and Wang Y 2006 A neuroinductive biomaterial based on dopamine *Proc. Natl Acad. Sci. USA* **103** 16681–6
[82] Zhou X, Cui H, Nowicki M, Miao S, Lee S J, Masood F, Harris B T and Zhang L G 2018 Three-dimensional-bioprinted dopamine-based matrix for promoting neural regeneration *ACS Appl. Mater. Interfaces* **10** 8993–9001
[83] Suuronen E J, Nakamura M, Watsky M A, Stys P K, Müller L J, Munger R, Shinozaki N and Griffith M 2004 Innervated human corneal equivalents as *in vitro* models for nerve-target cell interactions *FASEB J.* **18** 170–2
[84] Pollard R E, Mckay T B, Ford A, Cairns D M, Georgakoudi I and Kaplan D L 2020 Induction of irritation and inflammation in a 3D innervated tissue model of the human cornea *ACS Biomater. Sci. Eng.* **6** 6886–95
[85] Siran W *et al* 2018 Human corneal tissue model for nociceptive assessments *Adv. Healthcare Mater.* **7** 1800488